# Influence of chain length of gradient and block copoly(2-oxazoline)s on self-assembly and drug encapsulation

*Ondrej Sedlacek,[a,b] Valentin Bardoula,[a,c] Elina Vuorimaa-Laukkanen,[d] Lars Gedda,[e] Katarina Edwards,[e] Aurel Radulescu,[f] Grigoriy A. Mun,[g] Yong Guo,[h,i] Junnian Zhou,[i,j] Hongbo Zhang,[i] Véronique Nardello-Rataj,[c] Sergey Filippov,[g,i] Richard Hoogenboom[a,]**

O. Sedlacek, V. Bardoula, R. Hoogenboom

Supramolecular Chemistry Group, Department of Organic and Macromolecular Chemistry, Ghent University, Krijgslaan 281 S4, B-9000 Ghent, Belgium. E-mail: richard.hoogenboom@ugent.be

O. Sedlacek

Department of Physical and Macromolecular Chemistry, Faculty of Science, Charles University, Hlavova, 2030, 128 40 Prague 2, Czech Republic

V. Bardoula, V. Nardello-Rataj

Centrale Lille, Université de Lille, CNRS, Université Artois, UMR 8181-UCCS-Unité de Catalyse et Chimie du Solide, Lille, France

E. Vuorimaa-Laukkanen

Tampere University of Technology, Korkeakoulunkatu 7, 33720 Tampere, Finland

L. Gedda, K. Edwards

Department of Chemistry –Ångström Laboratory, Uppsala University, Lägerhyddsvägen 1, Uppsala, Sweden

A. Radulescu

Jülich Centre for Neutron Science (JCNS) at Heinz Maier-Leibnitz Zentrum (MLZ) Forschungszentrum Jülich GmbH, Lichtenbergstr. 1, 85748 Garching, Germany.

G. A. Mun, S. Filippov

Department of Chemistry & Technology of Organic Materials, Polymers and Natural Compounds, al Faraby Kazakh National University, 71, al-Faraby av., 050040, Almaty, Republic of Kazakhstan

S. Filippov
School of Pharmacy, University of Reading, Whiteknights, RG6 6DX Reading, United Kingdom

Y. Guo
Department of Endocrinology, Key Laboratory of National Health & Family Planning Commission for Male Reproductive Health, National Research Institute for Family Planning, Beijing 100081, China.

Y Guo, J. Zhou, H. Zhang
Pharmaceutical Sciences Laboratory and Turku Bioscience Center, of Åbo Akademi University and Turku Bioscience, Turku 20520, Finland

J. Zhou
Experimental Hematology and Biochemistry Lab, Beijing Institute of Radiation Medicine, Beijing 100850, China;

**Keywords:** gradient copolymers, poly(2-oxazoline)s, self-assembly, nanomedicine

**Abstract**

Amphiphilic gradient copolymers represent a promising alternative to extensively used block copolymers due to their facile one-step synthesis by statistical copolymerization of monomers of different reactivity. Herein, we provide an in-depth analysis of micelles based on amphiphilic gradient poly(2-oxazoline)s with different chain lengths to evaluate their potential for micellar drug delivery systems and compare them to the analogous diblock copolymer micelles. Size, morphology and stability of self-assembled nanoparticles, loading of hydrophobic drug curcumin, as well as cytotoxicities of the prepared nanoformulations were examined using copoly(2-oxazoline)s with varying chain lengths and comonomer ratios. In addition to several interesting differences between the two copolymer architecture classes, such as more compact self-assembled structures with faster exchange dynamics for the gradient copolymers, we can

conclude that gradient copolymers provide stable curcumin nanoformulations with comparable drug loadings to block copolymer systems and benefit from more straightforward copolymer synthesis. The study demonstrates the potential of amphiphilic gradient copolymers as a versatile platform for the synthesis of new polymer therapeutics.

## 1. Introduction

In the past decades, polymeric non-ionic surfactants emerged as essential materials for preparing diverse disperse systems with a broad range of applications.[1-4] Generally, they are represented by amphiphilic copolymers containing both hydrophilic and hydrophobic segments in the same chain.[5, 6] This amphiphilicity usually leads to their self-assembly in an aqueous environment into nanoparticles of various morphologies, such as micelles, cylindrical micelles and vesicles, with the first containing hydrophobic core stabilized by a hydrophilic shell. Micelles based on amphiphilic copolymers generally have higher colloidal stability than micelles based on low molar mass surfactants (e.g., sodium dodecyl sulfate).[7] Among the different amphiphilic copolymer architectures that can be used for the preparation of micelles, block copolymers are most commonly used due to their relatively easy synthesis, using a two-step sequential monomer addition procedure or the use of a preformed polymer as initiator. In the biomedical sciences, amphiphilic block copolymers are particularly useful for the solubilization of poorly water-soluble drugs, improving their maximal dosage and increasing their blood circulation times.[8] As an example, a nanoformulation of the anti-cancer drug paclitaxel encapsulated by poly(ethylene oxide)-block-poly(lactide) (PEO-PLA) copolymer micelles has been clinically approved for the treatment of metastatic breast cancer and advanced lung cancer in South Korea, distributed under the name Genexol®PM by Samyang Biopharm.[9]

Amphiphilic gradient copolymers represent an attractive alternative to block copolymers due to their even easier synthesis and tunable properties.[10-12] While the synthesis of block copolymers is essentially a multi-step process, gradient copolymers can be synthesized in a single step by statistical copolymerization of monomers with different reactivities, leading to a compositional drift in the formed copolymer.[13] The more reactive monomer is preferentially incorporated into the polymer chain at the beginning of the copolymerization process, while the less reactive one is preferentially incorporated at the end of copolymerization when the first monomer is being depleted. In the case of comonomers with substantially different reactivities, a copolymer with steep gradient architecture (quasi-block) is formed. Such behavior was observed in, e.g., radical copolymerization of (meth)acrylates and (meth)acrylamides with less reactive vinyl esters[14] or cyclic ketene acetals,[15] anionic

copolymerizations of functional epoxides,[16] aziridines,[17] styrene/isoprene pair[18] as well as the cationic ring-opening copolymerization (CROP) of different 2-alkyl-2-oxazolines[19-21] and 2-alkyl-2-oxazines.[22] Apart from the difference in monomer reactivities, the monomer distribution along the polymer chain can be controlled to a certain level by selecting the copolymerization temperature or solvent.[23] Finally, an important advantage of these spontaneously formed amphiphilic gradient copolymers over their block copolymer analogs is the possibility of fine-tuning the self-assembly properties by changing the steepness of the formed gradient as reported recently.[24]

Poly(2-alkyl-2-oxazoline)s (PAOx) are emerging polymers with rising potential in biomedical sciences.[25-27] Generally, they are synthesized by living cationic ring-opening polymerization (CROP) of 2-alkyl-2-oxazoline monomers leading to well-defined polymers with low molar mass dispersities.[28] The physical properties of PAOx mainly depend on the character of the side-chain substituent.[29] PAOx with short side-chain groups, i.e., poly(2-methyl-2-oxazoline) (PMeOx) and poly(2-ethyl-2-oxazoline) (PEtOx), are water-soluble biocompatible polymers that are particularly suitable for biomedical applications such as drug delivery systems or anti-fouling coatings.[30-32] On the other hand, PAOx with either aromatic or long aliphatic side-chains, e.g., poly(2-phenyl-2-oxazoline) (PPhOx) or poly(2-butyl-2-oxazoline) (PBuOx) are hydrophobic and found their application as core-forming blocks in amphiphilic copolymer nanoformulations.[33]

Several PAOx-based micellar drug delivery systems have been reported.[34, 35] Probably the most promising systems comprise PMeOx-PBuOx-PMeOx triblock copolymers, which allow encapsulation of an extremely high quantity (often > 50 wt.%) of hydrophobic drugs such as paclitaxel or curcumin.[33] These formulations show excellent anti-cancer properties both in vitro and in vivo.[36, 37] The main advantages of these systems are the simplicity of preparation and high drug loadings. The cost of the high drug loading is, however, the rapid diffusion-driven “burst release “of the drug from the micelle, which might lead to the premature loss of part of the cytostatic cargo before reaching the target tissue, which represents one of the major drawbacks of such systems. In our study, we use the PPhOx as a core-forming block due to its relative rigidity (glass transition temperature $T_g$ = 103–107 °C), as we assume that the rigid “glassy “ core could prevent the premature drug leakage compared to the flexible “liquid “ core of PBuOx.[29] Furthermore, the PPhOx-based micelles are expected to have higher stability, which can lead to their extended blood plasma circulation times.

Amphiphilic gradient PAOx can be synthesized in a single step by statistical copolymerization of more reactive 2-alkyl-2-oxazolines with less reactive 2-aryl-2-oxazolines.[29] As an example, different reactivities of MeOx and PhOx lead to the formation of an amphiphilic gradient PMeOx-grad-PPhOx copolymer that self-assembles in water into spherical or ellipsoid micelles.[19] The internal structure of these nanoparticles and their block analogs were thoroughly studied by various advanced scattering techniques, including small-angle X-ray scattering (SAXS) / small-angle neutron scattering (SANS) and light scattering. While the block copolymers assemble into micelles with uniform core density, the gradient copolymers form micelles with the outer part of the core denser than the center due to the chain back-folding, resulting in a smaller diameter of the gradient micelles compared to the block ones.[38] However, we anticipate that this behavior is chain-length dependent and a certain degree of polymerization (DP) is required to enable effective back-folding. Therefore, in this study, we introduce the use of polymer DP as an important parameter for the copolymer self-assembly and drug encapsulation, rather than a variation of the hydrophilic/hydrophobic unit ratio. Despite their indisputable potential, reports on the drug delivery systems based on amphiphilic gradient copolymers are still very sparse. Kronek et al. reported the encapsulation of the hydrophobic drug curcumin in amphiphilic gradient PEtOx-*grad*-poly(2-(4-dodecyloxyphenyl)-2-oxazoline) copolymer micelles.[39] The nanoformulations revealed decent drug-loading (12 – 22 wt.%), excellent in vitro stability and low toxicity. Very recently, Hruby et al. compared amphiphilic gradient and diblock copolymers of methyl-2-oxazoline (MeOx) with three different aromatic 2-oxazolines, having the total DP of 100.[40] At some comonomer ratios, the gradient copolymer based nanoformulations showed higher drug loadings than diblock analogs, which was hypothesized to result from a less dense micellar core structure. Despite the recent progress on the self-assembly and drug encapsulation by gradient copoly(2-oxazoline)s, all reported studies were limited to rather short polymer with a maximum DP of 100. As such, there is a lack of knowledge on the effect of the DP of gradient copolymers on their self-assembly and drug encapsulation behavior, which will be addressed for the first time in this work.

This study provides a detailed comparison of the micelles formed by the self-assembly of amphiphilic gradient and diblock copolymers, with systematical variation in their chain length, to assess their potential as drug-delivery vehicles. Therefore, we synthesized a series of amphiphilic PMeOx-PPhOx copolymers having the same hydrophilic/hydrophobic unit ratio while differing in the polymer architecture (gradient vs. diblock) and the total DP. The self-

assembly properties and the micelle dynamics were studied by several light-scattering techniques and Forster resonance energy transfer (FRET) spectroscopy to evaluate the effect of DP and monomer distribution on the self-assembly. Furthermore, different techniques were used for the encapsulation of the hydrophobic drug curcumin and the properties of the formed nanoformulations were critically compared and discussed in order to find an optimal architecture for micellar drug delivery systems.

## 2. Results and discussion

### 2.1. Copolymer synthesis

Amphiphilic gradient PMeOx-*grad*-PPhOx copolymers were synthesized in a one-step procedure using a microwave-assisted statistical CROP of MeOx and PhOx initiated by methyl *p*-toluenesulfonate in acetonitrile (**Figure 1**). Copolymers of two molar contents of MeOx ($F_{MeOx}$ = 0.6 or 0.7 corresponding to 46 wt% MeOx and 57 wt% MeOx, respectively) were prepared in different total chain lengths (DP 30, 40, 60, 80 100, 120, 150), labeled as $G_{60}$1-7 ($F_{MeOx}$ = 0.6) and G1-7 ($F_{MeOx}$ = 0.7). It was noted that the gradient copolymers with lower MeOx content ($G_{60}$1-7) showed reduced water-solubility, especially at higher total DPs. Therefore, the copolymers with higher MeOx content (G1-7) were used further for the direct comparison of block and gradient copolymers and a series of analogous block copolymers (B1-7) with the same MeOx content ($F_{MeOx}$ = 0.7) was synthesized in two steps by sequential polymerization of MeOx and PhOx. All copolymers were analyzed by $^1$H NMR spectroscopy, revealing the expected molecular composition. Size-exclusion chromatography revealed the formation of relatively well-defined copolymers with a narrow molar mass distribution ($Đ$ < 1.25). The size-exclusion chromatograms of the gradient and block copolymers with the same DP showed very good agreement, setting a solid ground for the comparison of their self-assembly behavior.

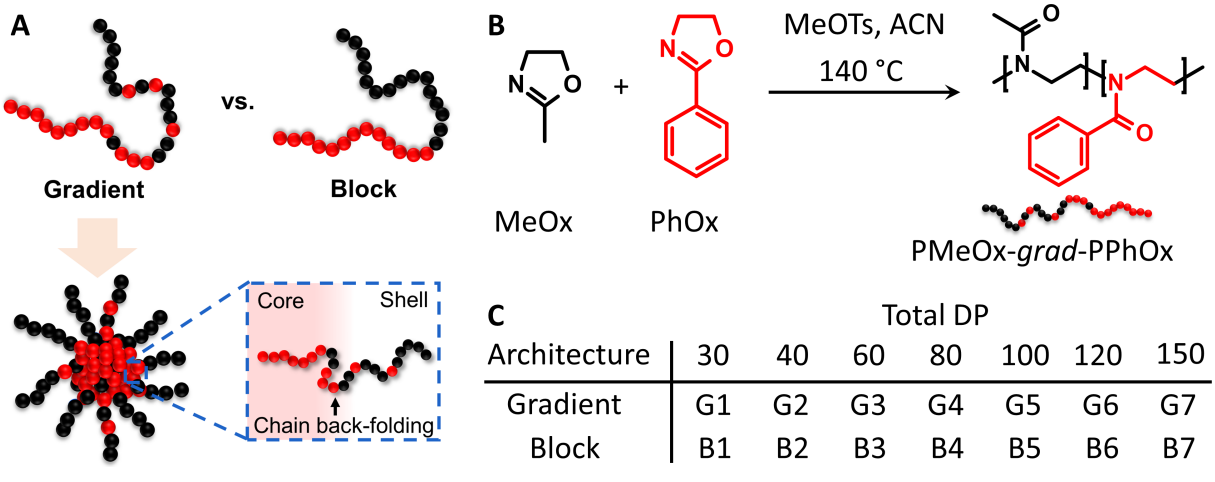


C

| Architecture | Total DP 30 | 40 | 60 | 80 | 100 | 120 | 150 |
|---|---|---|---|---|---|---|---|
| Gradient | G1 | G2 | G3 | G4 | G5 | G6 | G7 |
| Block | B1 | B2 | B3 | B4 | B5 | B6 | B7 |

**Figure 1**. Comparison of amphiphilic gradient and diblock copoly(2-oxazoline)s: Schematic illustration of both architectures (A). Synthesis of PMeOx-grad-PPhOx copolymers (B). Overview of the synthesized gradient (G1-G7), respectively diblock (B1-7) copolymers having the same MeOx:PhOx ratio of 70:30 (C).

### 2.2. Effect of copolymer architecture on self-assembly properties

All synthesized copolymers with $F_{MeOx}$ = 0.7 were water-dispersable and assembled into nanoparticles upon simple dissolution in water. The size of the nanoparticles was studied by dynamic light scattering (DLS, **Figure 2A, B**), revealing a significant effect of the total DP on the self-assembly behavior of the block and gradient copolymers. Shorter block and gradient copolymers with a DP below 60 resulted in micelles of nearly the same size. The formation of the large aggregates DP 30 can be ascribed to the composition heterogeneity within the individual copolymer chains. On the other hand, the micelles formed by the longer copolymers with a DP above 80 were found to be signficantly smaller for the gradient copolymers compared to the block copolymers, which is in agreement with our previous study on the comparison of block and gradient copolymer with DP 100.[19] From these results, it can be hypothesized that a minimal DP of 60 – 80 (i.e., 18-24 hydrophobic repeating units per chain) is required for efficient back-folding of the gradient copolymer chains, which leads to smaller nanoparticles. The size and morphology of the self-assembled structures were studied by cryogenic transmission electron microscopy (CryoTEM, **Figure 2C, S3**), corroborating the DLS data. The size of the nanoparticles increased with the total chain length. Gradient copolymer micelles showed a pure spherical morphology in the whole range of DPs. On the other hand, analogous block copolymer micelles showed a transition from spherical morphology at lower DPs to a mixture of spherical and worm-like morphology at higher DPs. This contributes to their bigger average size and broader dispersity, as observed by DLS, at higher DP than the gradient copolymer analogs since worm-like aggregates should have higher hydrodynamical diameter bringing additional polydispersity to size distribution. This transition from spherical to worm-like micelles can be ascribed to the increased interfacial tension from the longer hydrophobic blocks. For the gradient copolymer micelles, the absence of this morphological transition may be attributed to a denser core-shell transition region that protects these micelles from fusion in diluted solutions.

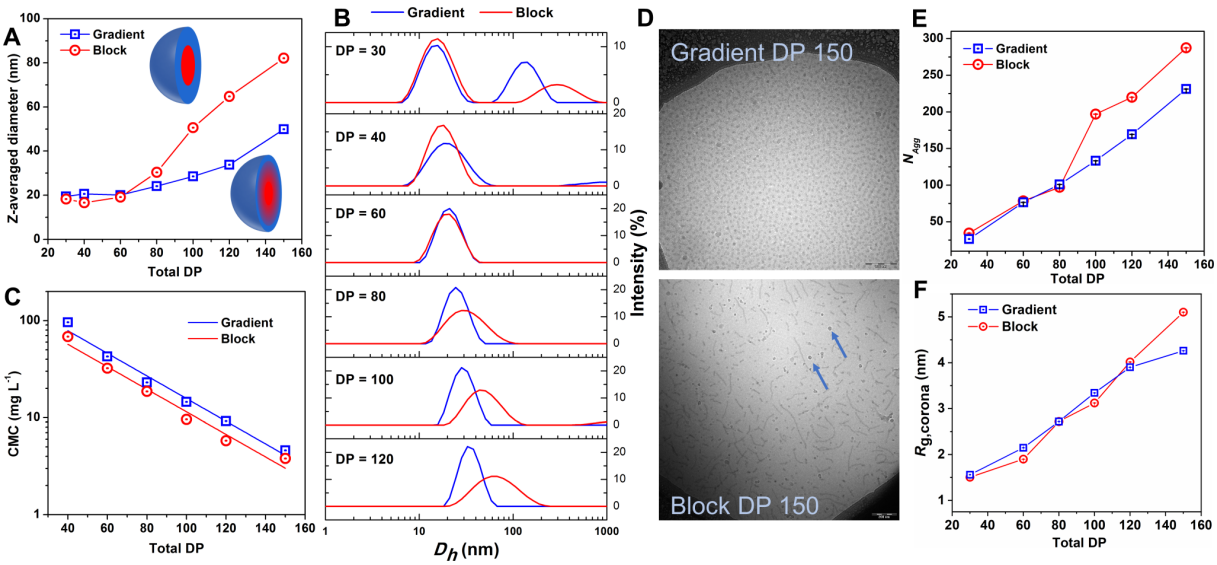


**Figure 2.** Comparison of self-assembly properties of PMeOx-PPhOx amphiphilic gradient and diblock copolymers ($F_{MeOx}$ = 0.7) in water. Hydrodynamic diameters (A) and size distributions of copolymers (B) in water ($c_{pol}$ = 10 mg mL$^{-1}$). Critical micelle concentrations (CMC) of the synthesized copolymers in water (C). CryoTEM images of G7 (top) and B7 (bottom) copolymers in water. Arrows indicate ice crystals artifacts. Scale bars represent 200 nm. (D). Aggregation number of copolymers in water as a function of DP (E). The gyration radius of a polymer chain in the nanoparticle corona as a function of polymerization degree (DP) of the copolymer micelles in water (F).

The structural characteristics of the B and G series of PMeOx-PPhOx micelles were also examined by small-angle neutron scattering (SANS; **Figure 2F** and Figure S4). The data were fitted using the block copolymer elliptical micelle model, which includes four structural parameters extracted from the model fitting to the data ($N_{agg}$, σ, $R_g$, and ε). From these fitting parameters, the micellar core radius ($R_{core}$) was calculated (Figure 2F). The low-$q$ region in the SANS data is most highly influenced by variations in the aggregation number ($N_{agg}$). $N_{agg}$ was extracted from the model and is shown in **Figure 2E**. We note that the gradient structure and molecular weight of the copolymers significantly impact the structural parameters of the micelles as will be discussed in the following.

The block copolymer micelle series showed a steeper increase in $N_{agg}$ with increasing copolymer molecular compared to the gradient copolymer micelles series $N_{agg}$ (**Table S4**), which is consistent with the trends observed by DLS and CryoTEM. It has previously been reported that $N_{agg}$ increases as the interfacial tension of the core−corona interface increases.[41] When the interfacial tension is high, the total interfacial area of the micelle system is decreased

by increasing $N_{agg}$, which also decreases the total number of micelles. In our system, varying the molecular weight and copolymer architecture tunes the core/corona interfacial tensions. $D_2O$ is a good solvent for PMeOx and a poor solvent for PPhOx; thus, as the hydrophobic block length increases, the interfacial tension and, respectively, $N_{agg}$ increases. The behavior observed in both block and gradient copolymer micelle series, in which $N_{agg}$ increased with increasing the length of the PPhOx block, is consistent with prior studies.[16] However, the gradient copolymer micelles exhibited a less pronounced increase of $N_{agg}$ as the copolymer molecular weight increased. We consider this as proof that the gradient structure impacts the core-corona interfacial tension due to the existence of additional interphase layers and loop formation.

The SANS experiments showed that spherical micelles are formed at low DP values below 60, whereas ellipsoidal micelles with eccentricity 1.1-2 are formed for copolymers with a DP above 80. This observation is not surprising since the asymmetry of PMeOx-PPhOx micelles was already reported previously.[16] The micellar asymmetry was explained by π-π stacking interactions of the phenyl rings in the PhOx block. Another interesting finding is the smaller $R_g$ value for hydrophilic corona in the gradient copolymer micelles series compared to the micelles of block copolymers with similar molecular weight and composition (Table S4). Such behavior can be explained by the loops that are formed in the PMeOx gradient copolymer micelles, resutling from hydrophobic PPhOx patches in between hydrophilic PMeOx parts. These loops will have a lower $R_g$ value in comparison with stretched polymer chains of the same length. Furthermore, the loops consist of a lower number of MeOx units, further reducing the $R_g$ value.

### 2.3. Effect of copolymer architecture on nanoparticle stability

The stability of the micelles plays a key role in the pharmacokinetic profile of the potential drug-loaded nanoformulations as more stable micelles will have longer blood circulation times and show slower non-specific leaching of encapsulated drugs.[42] On the other hand, micelles with extremely rigid, vitrified, cores show limited excretion and very slow drug release. In solution, self-assembled micelles theoretically exist in equilibrium with their unimers, if no kinetically trapped structures are formed. Upon dilution below their critical micelle concentration (CMC), such equilibrium micelles disassemble into unimers. Herein, the CMC of the prepared PMeOx-PPhOx copolymers was determined to assess the impact of the copolymer architecture and chain length on the equilibrium stability. The obtained CMC values ranged from 3.8 mg/L to 96 mg/L, which is in good agreement with previously reported data.[19]

Increasing the total length of the copolymers led to increased micelle stability, as indicated by lower CMC values (**Figure 2C, Tables S2 and S3**), corroborating previous reports.[43] This can be attributed to the larger interfacial tension of the micelles assembled from copolymers with longer hydrophobic segments. The block copolymer micelles are slightly more stable than the gradient analogs as indicated by slightly lower CMC values, which can be ascribed to the destabilization of the latter by the presence of a small fraction of hydrophilic units in the hydrophobic core.

The micelle-unimer exchange dynamics were studied by time-resolved Förster resonance energy transfer (FRET) of fluorescently labeled micelles (**Figures 3, S5, Table S5**). Two different micelle solutions of the same copolymers containing a minor fraction of covalently labeled copolymers functionalized with either a FRET donor (fluorescein) or a FRET acceptor (rhodamine B) were mixed and the fluorescence intensity of the acceptor (575 nm) was measured as function of time upon the excitation of the donor (455 nm). Directly after mixing there is no FRET emission, but when the labeled unimers start to exchange between the micelles the FRET emission increases due to the colocalization of the FRET donors and FRET acceptors within the same micelles. The increase in FRET emission in time was used to compare the dynamic stability of micelles prepared from gradient copolymer G5 and diblock copolymer B5. This fluorescence increase is rather small; however it is sufficient for the purpose of our experiment. The gradient copolymer micelles show a faster increase in FRET emission than the diblock copolymer analogs, presumably due to their higher CMC and, therefore, a higher concentration of unimers leading to faster unimer exchange between micelles. Alternatively, this observation could be explained in terms of the polymer residence time within the micelles, which, like the CMC, is governed by the free energy cost of dissolving the polymeric unimers in the aqueous phase. The measured increase in FRET intensity was fitted with a double exponential plot, revealing two distinct exchange rate constants for each system. This is likely related to the different relative hydrophilicity of the fluorescent labels. The acceptor molecule (rhodamine B) is more hydrophilic than the donor (fluorescein), which lowers the energetic barrier for the micelle-unimer equilibrium for the rhodamine B-labeled copolymers. These rhodamine-labeled unimers are then exchanged at a higher rate (with an exchange half-life ($t_{1/2}$) of 11 min for G5 and16 min for B5) than the fluorescein-labeled copolymers ($t_{1/2}$ = 146 min for G5, 218 min for B5). Based on these dynamic exchange experiments, it can be concluded that both G5 and B5 with DP 100 show dynamic unimer exchange and that the diblock copolymer micelles manifest higher stability than the gradient analogs. Besides the micelle-unimer

stability, other parameters might influence the stability of micelles in a biological environment, such as their interactions with serum proteins, which leads to their accelerated clearance of the micelles by the mononuclear phagocyte system. As these interactions depend mainly on the structure of the micelle shell, one might expect a difference between both copolymer architectures. However, this biological evaluation is beyond the scope of this article, focusing mainly on synthesis and physicochemical comparison of gradient and block copolymer nanoformulations.

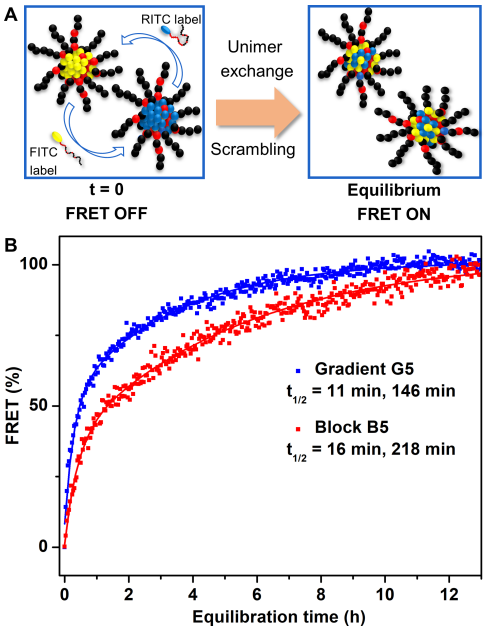


**Figure 3**. Dynamics of unimer exchange between fluorescently labeled micelles determined by the increase of the Förster resonance energy transfer (FRET) after mixing at 25 °C ($c_{pol}$ = 1 mg mL$^{-1}$). (A) Schematic illustration. (B) Comparison of the unimer exchange dynamics of G5 and B5.

### 2.4. Effect of copolymer architecture on hydrophobic drug loading

The drug solubilization ability of the prepared amphiphilic copolymers was investigated using curcumin as a model drug. In contrast to the study of Hruby and co-workers,[40] who loaded the micelles with relatively hydrophilic drug rifampicin (solubility in PBS reported as 9.9 mg mL$^{-1}$),[44] curcumin shows negligible solubility in water (<8 µg mL$^{-1}$),[45] and, therefore, represents an ideal model compound for our thorough encapsulation study that aims to enhance the soluble of hydrophobic drugs. Inspired by the ultra-high drug loading of poly(2-oxazoline) and poly(2-oxazine)s based micelles as reported by Kabanov and Luxenhofer, we first explored the thin-film rehydration approach (**Figure 4A**).[33, 35, 46, 47] Therefore, a solution of copolymer

(G1-G7 or B1-G7) and curcumin in ethanol was evaporated in a stream of air, forming a thin film in the vial. This film was then re-hydrated in PBS, which led to the formation of drug-loaded nanoparticles. As the solubility of curcumin in water is extremely low, the non-encapsulated or aggregated curcumin was removed by centrifugation. The amount of solubilized curcumin was measured by UV-VIS spectroscopy in ethanol (**Figure 4B, Table S6**). The final copolymer concentration was kept constant (10 mg/mL) while the curcumin feed was varied in the range from 1 mg $mL^{-1}$ to 4 mg $mL^{-1}$. The maximal drug loading (DL, the weight content of curcumin in the nanoformulation) that could be achieved was 16 wt.%. At low copolymer DPs and low curcumin feed, the loading efficiency (LE) was high and the amount of solubilized curcumin increased with curcumin feed. However, the highest curcumin feed (4 mg $mL^{-1}$) led to the formation of a water-insoluble polymer/curcumin precipitate due to the drug-polymer interactions and hydrophobization of the entire system. This effect was more pronounced for copolymers of higher DPs as well as for gradient copolymers compared to block copolymer analogs. Such behavior can be explained by the presence of a small quantity of hydrophobic PPhOx units in the hydrophilic PMeOx segments, which, in solid thin film blend, leads to increased inter-chain interactions, preventing efficient stabilization of the formed nanoparticles by the hydrophilic corona. As the thin film method was not very efficient for the preparation of curcumin-loaded gradient copolymer nanoformulations, other methods were explored that avoid the formation of a solid blend of curcumin with the copolymer.

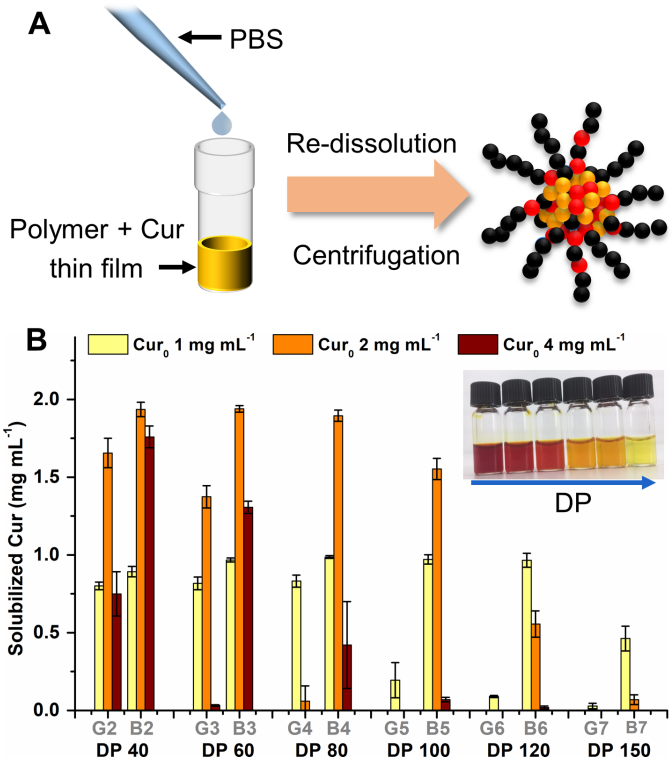

**Figure 4.** Solubilization of curcumin by PMeOx-PPhOx ($F_{MeOx}$ = 0.7) gradient (G2-G7) or diblock (B2-B7) copolymers using the thin-film hydration method. (A) Schematic illustration of the rehydration method for the preparation of the curcumin-loaded micelles. (B) Amount of curcumin solubilized by amphiphilic copolymers ($c_{pol}$ = 10 mg $mL^{-1}$) with the different feed of curcumin.

Stable nanoformulations of curcumin loaded amphiphilic copolymer micelles were obtained by the direct dissolution method. The surfactant properties of the amphiphilic copolymers in PBS (10 mg $mL^{-1}$) were used to directly solubilize the solid curcumin (12 mg $mL^{-1}$) upon heating and vortexing, leading to drug loadings around (DL) 15 wt.% (**Figure 5A,B, Table S7**), which is similar as observed for the rehydration method with low DP polymers. Interestingly, there was no significant difference in drug loadings between gradient, respectively block copolymer-based systems, nor for the copolymers with different DP above DP 60; only the very short polymers (DP 40) showed lower drug loading, presumably due to the lower stability of the DP 40 micelles. It can be assumed that the DL values obtained by direct dissolution depend on the ratio of hydrophobic/hydrophilic segments rather than the copolymer architecture. This was supported by a drug loading experiment using a gradient copolymer with a higher content of hydrophobic PPhOx ($G_{60}5$), which led to higher curcumin loading (18.1 wt.% compared to 15.0 wt.% for G5). . The size of the curcumin-loaded nanoparticles was slightly larger compared to drug-free micelles, as determined by DLS measurements (**Figure 5E,F,S7 Table S9**). Their morphology follows a similar pattern as observed for the unloaded micelles. All gradient copolymer-based formulations formed spherical micelles, while the block copolymer micelles formed a mixture of spherical and worm-like micelles in which the fraction of worm-like micelles increases with increasing copolymer DP.

Next, the stability of the G5 and B5-based curcumin nanoformulations was studied in solution (**Figure 5C**). A minor, insignificant, drop in curcumin content was observed after incubation of as-prepared nanoformulations at room temperature for 30 days, indicating excellent stability of the system, with no significant difference between gradient and block copolymer-based systems. For storage and transport purposes, the curcumin nanoformulations can be freeze-dried. The re-dissolution of the solid formulations obtained by the direct freeze-drying of G5, respectively B5-based nanoformulations led to the solutions containing nearly the same amount of solubilized curcumin as the samples before freeze-drying (**Figure 5D**). In

summary, direct drug loading proved as a superior method for loading curcumin into PMeOx-PPhOx copolymer nanoparticles. The only drawback consists in relatively longer encapsulation times (72 h) needed for saturation of micelles with curcumin. This can be partly eliminated by pre-dissolving the curcumin in a meager amount of DMSO. After adding the micelles solution in PBS, the curcumin forms a fine suspension that is quickly uptaken by nanoparticles, reducing the encapsulation time to less than 30 min. The drug loadings obtained by this method were similar to the values obtained by the DMSO-free method (**Figure S6**). The relative content of DMSO in nanoformulations is low (<3% v/v). Finally, a popular nanoprecipitation method was used to prepare curcumin-loaded nanoformulations, resulting in slightly higher drug loadings (ca 16 wt.%, **Table S8**). Herein, a mixture of the copolymer with curcumin was nanoprecipitated from ethanol into PBS, followed by ethanol evaporation under vacuum. However, extreme care has to be taken during the evaporation process to avoid the formation of the dry, thin-film, which leads to a sparingly soluble precipitate as described above.

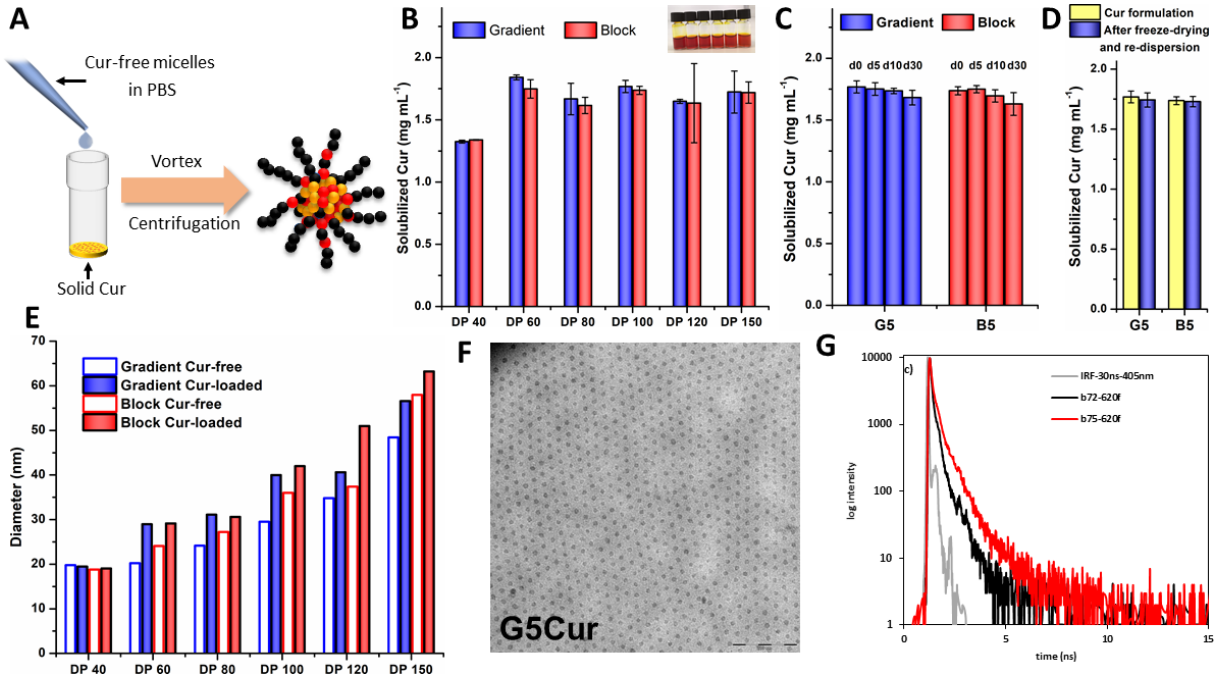


**Figure 5.** Solubilization of curcumin by PMeOx-PPhOx ($F_{MeOx}$ = 0.7) gradient (G2-G7) or diblock (B2-B7) copolymers using the direct dissolution method. (A) Schematic illustration of the loading of curcumin in preformed micelles. (B) The maximal amount of curcumin solubilized by amphiphilic copolymers ($c_{pol}$ = 10 mg mL$^{-1}$) in PBS using an excess feed of curcumin (12 mg mL$^{-1}$). (C) Stability of G5, respectively B5 curcumin nanoformulations in PBS 5, 10 and 30 days after loading. (D) Amount of curcumin solubilized by G5, respectively B5, before and after freeze-drying and re-dispersion ($c_{pol}$ = 10 mg mL$^{-1}$). (E) The hydrodynamic

diameter of the G2-G7, respectively B2-B7 nanoparticles before and after curcumin loading ($c_{pol}$ = 10 mg mL$^{-1}$). (F) Cryo-TEM image of curcumin-loaded G5 nanoparticles (scale bar 200 nm). (G) Fluorescence decay curves for curcumin-loaded G5 and B5 with $\lambda_{ex}$ = 405 nm, the decays were monitored at 620 nm.

To conclude, the direct dissolution of curcumin by an aqueous gradient or block copolymer solution provides straightforward access to nanoformulations with decent loading of a hydrophobic drug. For instant clinical application, pre-dissolving curcumin in a small amount of DMSO leads to the nanoformulations in a short time (< 30 min). When storage of the solid freeze-dried nanoparticles is needed, the direct dissolution of solid curcumin by the copolymer micelles is preferred, however, at the cost of a longer encapsulation time. These DMSO-free samples were then used for further investigations, from now on abbreviated as, e.g., B5Cur, G5Cur and $G_{60}$5Cur representing nanoformulations based on copolymer B5, G5 respectively $G_{60}$5. Interestingly, we have shown that the copolymer architecture does not play a significant role in the maximal curcumin loading, as both gradient and diblock analogs show similar drug loadings. These results are in line with the recently published study by Hruby et al.[40] On the other hand, the drug loading can be improved by increasing the amount of PPhOx in the copolymer. This suggests that the curcumin loading depends on the hydrophobic/hydrophilic ratio of the amphiphilic copolymers rather than the monomer distribution or chain length.

**2.5. Spectroscopic characteristics of nanoformulations**

Six formulations were selected for the spectroscopic studies of the curcumin-loaded micelles, namely B2Cur, G2Cur, and $G_{60}$2Cur (DP 40) as well as B5Cur, G5Cur, and $G_{60}$5Cur (DP 100). Two examples of the absorption spectra for the micelles in PBS are shown in **Figure S8A**. In aqueous buffers, the absorption spectra of free curcumin exhibit a characteristic broad peak at 430 nm and a small shoulder at 355 nm. In the PMeOx-PPhOx micelles, the broad peak around 430 nm becomes prominent, and the shoulder peak at 355 nm disappears with the appearance of a new shoulder at 450 nm. These changes in the absorption spectrum indicate that curcumin is in a nonpolar-like environment. Minor differences in the maximum absorption wavelength were observed for the present samples (**Table S10**). For DP = 40, the absorption maximum is always at 2-4 nm shorter wavelength as for the corresponding DP = 100 system, whereas for the MeOx molar content of 0.7, the absorption maximum is at ~5 nm shorter wavelength than for 0.6. The absorption spectra for the corresponding block polymer and

gradient polymer were equal, implying that curcumin is not entirely buried inside the PPhOx core but interacts with water.

In a nonpolar environment, the fluorescence spectrum of curcumin blue-shifts to 500 nm compared to 550 nm in an aqueous solution. However, the fluorescence spectra of the curcumin-loaded micelles (**Figure S8B**) exhibit a considerable red shift having their maxima close to 620 nm. This can be explained by the well-known keto−enol tautomerism of curcumin, which induces aggregation and causes a significant decrease in the fluorescence intensity accompanied by a red-shifted fluorescence. The micelles with DP = 100 have higher relative fluorescence efficiency, $\varphi_{rel}$ , and their fluorescence maximum is at shorter wavelengths than those with DP = 40. This could indicate that curcumin is more aggregated in the micelles resulting from shorter copolymers with DP 40 and/or in a more polar environment. For the systems based on copolymers with a MeOx molar content of 0.7, the $\varphi_{rel}$ is lower than for corresponding micelles with a MeOx molar content of 0.6. Also, the block copolymer micelles have higher relative fluorescence efficiency than the corresponding gradient polymer.

The fluorescence decays of curcumin measured for the selected formulations show a multiexponential behavior (**Figure S8C**). This is typical for curcumin systems since its fluorescence lifetime varies with changes in, for example, viscosity, polarity, and hydrogen-bonding ability of the environment. In the present study, the lifetime values were obtained by fitting the decays with the three-exponential decay model (eq S1) (and are tabulated in **Table S10**). The shortest ~100 ps component dominates the decays with ~10-20 % contribution of the ~450 ps component. The proportion of the longest-living 0.8 - 1.5 ns component is very small (~0.1%), but without its presence, it was not possible to obtain acceptable fitting results. This minor population could represent small amounts of monomeric curcumin molecules in a highly nonpolar environment. The observed complex fluorescence decay curves suggest a local heterogeneity in the distribution and degree of aggregation of the curcumin inside the micelles. When comparing the different formulations, it is simpler to consider the average fluorescence lifetimes <τ> (**Table S10**) instead of emphasizing all the decay components. The <τ> is shorter for systems based on copolymers with a MeOx molar content of 0.7 than for corresponding micelles with a MeOx molar content of 0.6. Also, <τ> are ~50 ps longer for micelles based on copolymers with a DP of 100 compared to polymers with a DP of 40. As a summary, the spectroscopic studies of the curcumin-loaded micelles indicate that in micelles based on copolymers with a DP of 100 the curcumin is more shielded from the polar environment than in the micelles based on copolymers with a DP of 40. Also, according to the fluorescence

measurements, there is a small difference between the block polymer and gradient copolymer micelles: either the curcumin is less aggregated or better shielded in the block copolymer micelles.

### 2.6. In vitro drug release

The release of curcumin from the nanoformulations was studied in PBS at 37 °C using a dialysis method. A relatively high molecular weight cut-off dialysis membrane (50 kDa) was selected to mimic the sink conditions in vivo and ensure the rapid permeability of both released curcumin and macromolecular unimers. Generally, two main mechanisms contribute to the drug release from the micellar formulation. In the beginning, the diffusion-driven leaching of the drug from the outer parts of the core results in so-called "burst release ", which leads to the rapid loss of a significant part of the drug cargo. This is considered one of the main drawbacks of micellar nanoformulation systems.[48] After this initial release, the remaining drug is trapped inside the hydrophobic core and the diffusion-driven release is slowed down. At this moment, the micelle disassembly, due to the micelle-unimer equilibrium, mostly drives the drug release. From the biomedical point of view, the ideal micellar system should combine low burst drug release with sustained release afterward. Comparing the curcumin release from the synthesized gradient and block copolymer nanoformulations G2Cur, B2Cur, G5Cur, and B5Cur revealed a relatively small burst release (ca 12% of curcumin released after 2 h of incubation), which is statistically independent of the copolymer architecture and length. This can be explained by several factors, such as the rigidity of the micellar core, interactions between curcumin and the aromatic core, as well as the relatively low drug loading. On the other hand, upon longer incubation times, faster drug release was observed from the gradient copolymer formulations, presumably due to their lower stability. This corroborates the fact that the less stable shorter-DP micelles release curcumin faster than their longer polymer analogs. The faster sustained drug release from the gradient copolymer nanoformulations might be beneficial for the pharmacokinetic profile of the carried drug.

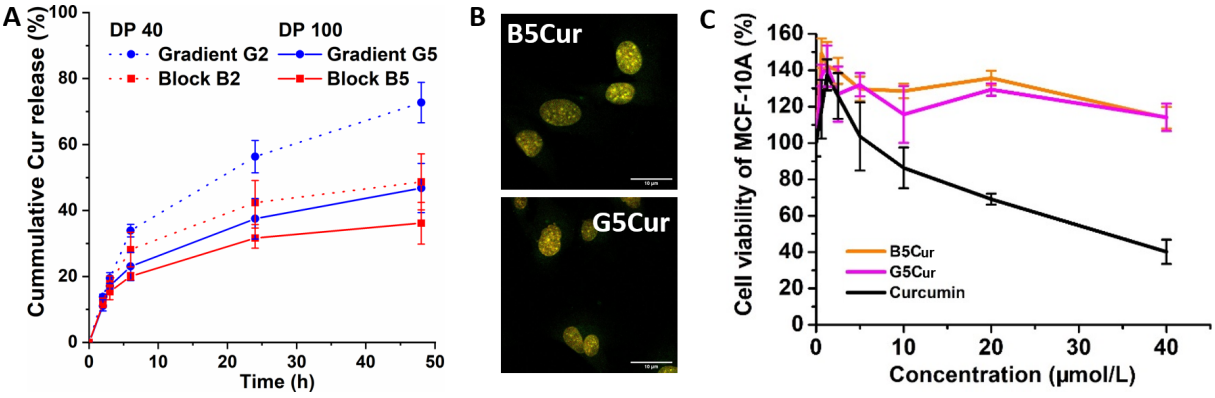


**Figure 6.** (A) Release of curcumin from micellar nanoformulations in PBS (pH = 7.4, 37 °C). (B) Uptake of curcumin nanoformulations B5Cur, respectively G5Cur into MDA-MB-231 cells after 2 h of incubation. Scale bars represent 10 µm. (C) Viability of MCF-10A cells after 48 h incubation with nanoformulations loaded by B5Cur or G5Cur and free curcumin, respectively. The concentrations refer to curcumin content.

### 2.7. In vitro biological evaluation

For application as drug delivery vehicles, the nanoformulations should be rapidly internalized by cells. This was confirmed by confocal microscopy, which confirmed the rapid internalization of the curcumin-loaded nanoformulations G5Cur and B5Cur by MDA-MB-231 cells upon short incubation times (2 h, **Figure 6B**). Furthermore, the cytotoxicity of G5Cur, B5Cur, and free curcumin was evaluated by an *in vitro* experiment using normal breast MCF-10A cells and breast cancer MDA-MB-231 cells respectively (**Figure 6C, S9**). The cells were incubated in the presence of the copolymer nanoformulations for 48 h at 37 °C, after which the cell viability was assessed by WST-1 assay. The results showed that in MCF-10A cells, curcumin-loaded B5C and curcumin-loaded G5C have no cytotoxicity, while the free curcumin has significant cytotoxicity with increasing concentration ($P < 0.0001$). On the other hand, MDA-MB-231 cells are less sensitive to free curcumin. Within the studied concentration range, free curcumin, as well as curcumin-loaded B5C and G5C, show very similar cytotoxicity profiles, with signs of cytotoxicity observed only for the highest concentrations tested. These results suggest that there are no significant differences between both curcumin-loaded B5C and G5C and underline the potential of amphiphilic gradient copolymers as drug delivery vehicles.

## 3. Conclusions

In summary, we studied aqueous self-assembly and hydrophobic drug encapsulation of a series of amphiphilic gradient copoly(2-oxazoline)s with different chain lengths and compared them to diblock copolymer analogs. We observed strong dependence of the self-assembly characteristics on the total polymer length. While shorter block and gradient copolymers with a DP below 60 self-assembled into micelles of nearly the same size, the micelles formed by the longer copolymers were found to be smaller for the gradient copolymers compared to the block copolymers. The stability of the nanoparticles showed chain length dependence, with gradient copolymer micelles being more dynamic and slightly less stable than block analogs but still sufficiently stable for intended biomedical applications. The potential of the prepared copolymers as drug delivery systems was thoroughly examined using model drug curcumin. Three different methods for drug-loaded nanoformulations fabrication were studied, where the direct encapsulation of solid curcumin by pre-assembled micelles provided the best results. The prepared nanoformulations were stable upon storage, showed significant cellular uptake and cytotoxicity. Interestingly, there were no significant differences between the maximal drug loadings of analogous gradient and diblock copolymer nanoparticles. Considering their straightforward single-step synthesis, gradient copolymer nanoformulations represent an attractive alternative to block copolymer amphiphiles for the construction of novel drug delivery systems. To fully evaluate their biomedical potential, further biological assessment of gradient copolymer nanoparticles will be necessary, including in vivo toxicity, pharmacokinetics and therapeutic effectivity.

**Supporting Information**

Supporting Information is available from the Wiley Online Library or from the author: Full experimental procedures, characterization of polymers, polymer nanoparticles and drug-loaded nanoparticle formulations.

**Acknowledgements**

RH thanks FWO and Ghent University for continuous financial support. O.S. thanks the funding from the FWO and European Union's Horizon 2020 research and innovation program under the Marie Skłodowska-Curie grant agreement No 665501. S.F. acknowledges the Leverhulme Trust for the visiting professorship grant (VP2-2020-013) to support the visit and work of S.F. at the University of Reading.

Received: ((will be filled in by the editorial staff))
Revised: ((will be filled in by the editorial staff))
Published online: ((will be filled in by the editorial staff))

**References**

[1] Tonge, S.; Tighe, B., *Advanced drug delivery reviews* **2001,** *53* (1), 109-122.

[2] Garnier, S.; Laschewsky, A., *Langmuir* **2006,** *22* (9), 4044-4053.

[3] Letchford, K.; Burt, H., *European journal of pharmaceutics and biopharmaceutics* **2007,** *65* (3), 259-269.

[4] Uchegbu, I. F.; Vyas, S. P., *International journal of pharmaceutics* **1998,** *172* (1-2), 33-70.

[5] Mai, Y.; Eisenberg, A., *Chemical Society Reviews* **2012,** *41* (18), 5969-5985.

[6] Blanazs, A.; Armes, S. P.; Ryan, A. J., *Macromolecular rapid communications* **2009,** *30* (4‐5), 267-277.

[7] Nakashima, K.; Bahadur, P., *Advances in colloid and interface science* **2006,** *123*, 75-96.

[8] Kataoka, K.; Harada, A.; Nagasaki, Y., *Advanced drug delivery reviews* **2012,** *64*, 37-48.

[9] Hare, J. I.; Lammers, T.; Ashford, M. B.; Puri, S.; Storm, G.; Barry, S. T., *Advanced drug delivery reviews* **2017,** *108*, 25-38.

[10] Chen, Y.; Chen, H.; Feng, M.; Dong, Y., *European Polymer Journal* **2016,** *85*, 489-498.

[11] Alam, M. M.; Jack, K. S.; Hill, D. J.; Whittaker, A. K.; Peng, H., *European Polymer Journal* **2019,** *116*, 394-414.

[12] Deng, Z.; Shi, Q.; Tan, J.; Hu, J.; Liu, S., *ACS Materials Letters* **2021,** *3* (9), 1339-1356.

[13] Zhang, J.; Farias‐Mancilla, B.; Destarac, M.; Schubert, U. S.; Keddie, D. J.; Guerrero‐Sanchez, C.; Harrisson, S., *Macromolecular Rapid Communications* **2018,** *39* (19), 1800357.

[14] Yañez-Macias, R.; Kulai, I.; Ulbrich, J.; Yildirim, T.; Sungur, P.; Hoeppener, S.; Guerrero-Santos, R.; Schubert, U. S.; Destarac, M.; Guerrero-Sanchez, C., *Polymer Chemistry* **2017,** *8* (34), 5023-5032.

[15] Agarwal, S., *Polymer Chemistry* **2010,** *1* (7), 953-964.

[16] Gleede, T.; Rieger, E.; Blankenburg, J.; Klein, K.; Wurm, F. R., *Journal of the American Chemical Society* **2018,** *140* (41), 13407-13412.

[17] Gleede, T.; Markwart, J. C.; Huber, N.; Rieger, E.; Wurm, F. R., *Macromolecules* **2019,** *52* (24), 9703-9714.

[18] Galanos, E.; Grune, E.; Wahlen, C.; Müller, A. H.; Appold, M.; Gallei, M.; Frey, H.; Floudas, G., *Macromolecules* **2019,** *52* (4), 1577-1588.

[19] Filippov, S. K.; Verbraeken, B.; Konarev, P. V.; Svergun, D. I.; Angelov, B.; Vishnevetskaya, N. S.; Papadakis, C. M.; Rogers, S.; Radulescu, A.; Courtin, T.; Martins, J. C.; Starovoytova, L.; Hruby, M.; Stepanek, P.; Kravchenko, V. S.; Potemkin, I. I.; Hoogenboom, R., *J Phys Chem Lett* **2017,** *8* (16), 3800-3804. DOI 10.1021/acs.jpclett.7b01588.

[20] Lambermont‐Thijs, H. M.; Jochems, M. J.; Hoogenboom, R.; Schubert, U. S., *Journal of Polymer Science Part A: Polymer Chemistry* **2009,** *47* (23), 6433-6440.

[21] Hoogenboom, R.; Fijten, M. W.; Wijnans, S.; van den Berg, A. M.; Thijs, H. M.; Schubert, U. S., *Journal of combinatorial chemistry* **2006,** *8* (2), 145-148.

[22] Sedlacek, O.; Lava, K.; Verbraeken, B.; Kasmi, S.; De Geest, B. G.; Hoogenboom, R., *Journal of the American Chemical Society* **2019,** *141* (24), 9617-9622.

[23] Van Steenberge, P. H.; Verbraeken, B.; Reyniers, M.-F. o.; Hoogenboom, R.; D'hooge, D. R., *Macromolecules* **2015,** *48* (21), 7765-7773.

[24] Bera, D.; Sedlacek, O.; Jager, E.; Pavlova, E.; Vergaelen, M.; Hoogenboom, R., *Polymer Chemistry* **2019,** *10* (37), 5116-5123.

[25] Hoogenboom, R., *Angewandte Chemie International Edition* **2009,** *48* (43), 7978-7994.

[26] Schlaad, H.; Diehl, C.; Gress, A.; Meyer, M.; Demirel, A. L.; Nur, Y.; Bertin, A., *Macromolecular rapid communications* **2010,** *31* (6), 511-525.

[27] Lorson, T.; Lübtow, M. M.; Wegener, E.; Haider, M. S.; Borova, S.; Nahm, D.; Jordan, R.; Sokolski-Papkov, M.; Kabanov, A. V.; Luxenhofer, R., *Biomaterials* **2018,** *178*, 204-280.

[28] Verbraeken, B.; Monnery, B.; Lava, K.; Hoogenboom, R., *European Polymer Journal* **2017,** *88*, 451-469.

[29] Glassner, M.; Vergaelen, M.; Hoogenboom, R., *Polymer International* **2018,** *67* (1), 32-45.

[30] Morgese, G.; Verbraeken, B.; Ramakrishna, S. N.; Gombert, Y.; Cavalli, E.; Rosenboom, J. G.; Zenobi‐Wong, M.; Spencer, N. D.; Hoogenboom, R.; Benetti, E. M., *Angewandte Chemie International Edition* **2018,** *57* (36), 11667-11672.

[31] Sedlacek, O.; Hoogenboom, R., *Advanced Therapeutics* **2020,** *3* (1), 1900168.

[32] Sedlacek, O.; Van Driessche, A.; Uvyn, A.; De Geest, B. G.; Hoogenboom, R., *Journal of Controlled Release* **2020,** *326*, 53-62. DOI https://doi.org/10.1016/j.jconrel.2020.06.018.

[33] Luxenhofer, R.; Schulz, A.; Roques, C.; Li, S.; Bronich, T. K.; Batrakova, E. V.; Jordan, R.; Kabanov, A. V., *Biomaterials* **2010,** *31* (18), 4972-4979.

[34] He, Z.; Schulz, A.; Wan, X.; Seitz, J.; Bludau, H.; Alakhova, D. Y.; Darr, D. B.; Perou, C. M.; Jordan, R.; Ojima, I., *Journal of controlled release* **2015,** *208*, 67-75.

[35] Lübtow, M. M.; Hahn, L.; Haider, M. S.; Luxenhofer, R., *Journal of the American Chemical Society* **2017,** *139* (32), 10980-10983.

[36] He, Z.; Wan, X.; Schulz, A.; Bludau, H.; Dobrovolskaia, M. A.; Stern, S. T.; Montgomery, S. A.; Yuan, H.; Li, Z.; Alakhova, D.; Sokolsky, M.; Darr, D. B.; Perou, C. M.; Jordan, R.; Luxenhofer, R.; Kabanov, A. V., *Biomaterials* **2016,** *101*, 296-309. DOI https://doi.org/10.1016/j.biomaterials.2016.06.002.

[37] Wan, X.; Beaudoin, J. J.; Vinod, N.; Min, Y.; Makita, N.; Bludau, H.; Jordan, R.; Wang, A.; Sokolsky, M.; Kabanov, A. V., *Biomaterials* **2019,** *192*, 1-14. DOI https://doi.org/10.1016/j.biomaterials.2018.10.032.

[38] Kravchenko, V. S.; Potemkin, I. I., *The Journal of Physical Chemistry B* **2016,** *120* (47), 12211-12217. DOI 10.1021/acs.jpcb.6b10120.

[39] Datta, S.; Jutková, A.; Šrámková, P.; Lenkavská, L.; Huntošová, V.; Chorvát, D.; Miškovský, P.; Jancura, D.; Kronek, J., *Biomacromolecules* **2018,** *19* (7), 2459-2471. DOI 10.1021/acs.biomac.8b00057.

[40] Loukotová, L.; Švec, P.; Groborz, O.; Heizer, T.; Beneš, H.; Raabová, H.; Bělinová, T.; Herynek, V.; Hrubý, M., *Macromolecules* **2021**. DOI 10.1021/acs.macromol.0c02674.

[41] Lund, R.; Willner, L.; Stellbrink, J.; Radulescu, A.; Richter, D., *Macromolecules* **2004,** *37* (26), 9984-9993.

[42] Cabral, H.; Miyata, K.; Osada, K.; Kataoka, K., *Chemical reviews* **2018,** *118* (14), 6844-6892.

[43] Chen, L. G.; Bermudez, H., *Langmuir* **2012,** *28* (2), 1157-1162. DOI 10.1021/la2040399.

[44] Florey, K., *Analytical Profiles of Drug Substances, Volume 5*. Elsevier Science & Technology: **1976**.

[45] Suresh, K.; Nangia, A., *CrystEngComm* **2018,** *20* (24), 3277-3296. DOI 10.1039/C8CE00469B.

[46] He, Z.; Wan, X.; Schulz, A.; Bludau, H.; Dobrovolskaia, M. A.; Stern, S. T.; Montgomery, S. A.; Yuan, H.; Li, Z.; Alakhova, D., *Biomaterials* **2016,** *101*, 296-309.

[47] Lübtow, M. M.; Haider, M. S.; Kirsch, M.; Klisch, S.; Luxenhofer, R., *Biomacromolecules* **2019,** *20* (8), 3041-3056.

[48] Liu, J.; Lee, H.; Allen, C., *Current pharmaceutical design* **2006,** *12* (36), 4685-4701.

We provide an in-depth analysis of micelles based on amphiphilic gradient poly(2-oxazoline)s with different chain lengths to evaluate their potential for micellar drug delivery systems and compare them to the analogous diblock copolymer micelles. In addition to several interesting differences between the two copolymer architecture classes, we can conclude that gradient copolymers provide stable nanoformulations with comparable drug loadings to block copolymer systems and benefit from more straightforward copolymer synthesis.

O. Sedlacek, V. Bardoula, E. Vuorimaa-Laukkanen, L. Gedda, K. Edwards, A. Radulescu, G. A. Mun,. Y. Guo, J. Zhou, H. Zhang, V. Nardello-Rataj, S. Filippov, R. Hoogenboom*

**Influence of chain length of gradient and block copoly(2-oxazoline)s on self-assembly and drug encapsulation**

ToC figure:

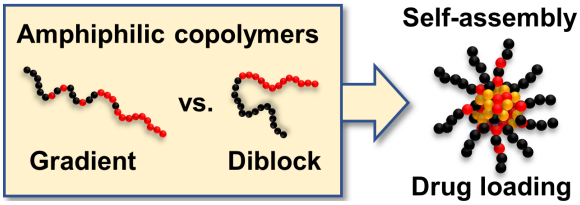


# Supporting Information

**Influence of chain length of gradient and block copoly(2-oxazoline)s on self-assembly and drug encapsulation**

*Ondrej Sedlacek,[a,b] Valentin Bardoula,[a,c] Elina Vuorimaa-Laukkanen,[d] Lars Gedda,[e] Katarina Edwards,[e] Aurel Radulescu,[f] Grigoriy A. Mun,[g] Yong Guo,[h,i] Junnian Zhou,[i,j] Hongbo Zhang,[i] Véronique Nardello-Rataj,[c] Sergey Filippov,[g,i] Richard Hoogenboom[a,]**

**Materials**

2-Methyl-2-oxazoline (MeOx) and 2-phenyl-2-oxazoline (PhOx) were obtained from Acros Organics and Sigma-Aldrich, respectively, and were distilled from barium oxide prior to use.

Methyl *p*-toluenesulfonate (MeOTs) was obtained from Sigma-Aldrich and was distilled from calcium hydride prior to use. Acetonitrile (Sigma-Aldrich) was purified over aluminum oxide using a solvent purification system from J.C. Meyer. Curcumin (≥98%) was obtained from Across Chemicals (product code 10286890). All other chemicals, including piperazine, fluorescein isothiocyanate (FITC), rhodamine B isothiocyanate (RITC), triethylamine and phosphate buffer-saline tablets were purchased from Sigma-Aldrich and were used as received. Water was deionized with a Millipore Milli-Q water purification system.

**Instrumentation**

All stock solutions and samples were prepared in a VIGOR Sci-Lab SG 1200/750 *glovebox system* with a water concentration ≤ 0.1 ppm. For the polymerizations, a Biotage Initiator EXP *microwave system* with Robot Sixty was used. *Gas chromatography (GC)* was used to monitor the kinetics of the CROP employing an Agilent 7890A system equipped with a VWR Carrier-160 hydrogen generator and an Agilent HP-5 column of 30 m length and 0.32 mm diameter. An FID detector was used, and the inlet was set to 240 °C with a split injection ratio 25:1. Hydrogen was used as carrier gas at a flow rate of 2 mL $min^{-1}$ *Size exclusion chromatography (SEC)* was used to determine the molecular weights ($M_w$ - mass-averaged molecular weight, $M_n$ - number-averaged molecular weight) and the dispersity ($Đ = M_m/M_n$) of the prepared polymers. This was performed using an Agilent 1260-series HPLC system equipped with a 1260 ISO-pump, a 1260 automatic liquid sampler, a thermostatted column compartment at 50 °C equipped with two PLgel 5 μm mixed-D columns and a precolumn in series, a 1260 diode array detector 1260 RI detector and multi-angle light scattering detector (Wyatt miniDawn Treos II). The used eluent was DMA containing 50 mM of LiCl at a flow rate of 0.5 ml $min^{-1}$. Molar mass values and *Đ* values are calculated using narrow-dispersity PEtOx standards. *Nuclear magnetic resonance (NMR)* spectra were measured with a Bruker Advance MSL 400 MHz NMR spectrometer. All chemical shifts are given in ppm. *Dynamic light scattering (DLS) measurements were* used to measure hydrodynamic diameters ($D_h$) of prepared polymers using a Zetasizer NanoZS instrument, Model ZEN3600 (Malvern Instruments, UK). The polymer samples were prepared in Mili-Q water or PBS by direct dissolution and were filtered prior to measurement through a 0.22 μm PTFE filter. Due to the possible multimodal peak distribution, the volume-weighted mean $D_h$ was determined at a scattering angle of θ = 173° and the DTS (Nano) program was used to evaluate the data. The volume distribution was derived from the intensity distribution using Mie theory.

**Copolymer synthesis**

For the synthesis of the *gradient copolymers*, the respective monomers (MeOx and PhOx) were mixed with acetonitrile in the desired molar ratio in microwave vial; the total monomer concentration was 3 M in all cases. The calculated amount of MeOTs initiator was added, the monomer to initiator ratio varied from 30 (for copolymer G1) to 150 (for copolymer G7). As a representative example, the solution for copolymer G5 (target DP=100) was obtained by mixing of MeOx (3.21 g, 37.8 mmol), PhOx (2.71 g, 16.2 mmol), acetonitrile (12.1 mL) and MeOTs (81.4 µL, 0.54 mmol). The vials were sealed and polymerized at 140 °C in a microwave reactor for times indicated in Table S1. The analogous *block copolymers* were prepared in a similar way by sequential copolymerization of both monomers, starting with MeOx. After the polymerization of the first block, the vial was transferred into the glovebox and the second monomer (PhOx) and a part of acetonitrile were added. The vial was again closed and the second block was polymerized as described above. After the polymerization, the copolymers were terminated with methanolic KOH (1 M, 3 eq) for 2 h at room temperature and isolated by precipitation in cold diethyl ether, followed by filtration and drying under reduced pressure. $^{1}$H NMR spectra of copolymers were recorded in DMSO-*d6*. The copolymer composition was calculated from the ratio of the aromatic PPhOx protons (6.8-7.6 ppm) and the aliphatic -$CH_3$ protons of PMeOx (2 ppm). Before further use, these samples were further dried under reduced pressure to remove all monomer traces. Molecular weights and dispersity (*Đ*) values were measured by SEC in DMA.

**Table S1**. Polymerization times for G1-7, respectively B1-7 copolymers at 140 °C.

| Copolymer | Polymerization time (min) | Copolymer | Polymerization time 1. block (min) | Polymerization time 2. block (min) |
|---|---|---|---|---|
| G1 | 18 | B1 | 3.1 | 18 |
| G2 | 24 | B2 | 4.2 | 24 |
| G3 | 36 | B3 | 6.3 | 36 |
| G4 | 48 | B4 | 8.3 | 48 |
| G5 | 60 | B5 | 10.4 | 60 |
| G6 | 72 | B6 | 12.5 | 72 |
| G7 | 90 | B7 | 15.6 | 90 |

**Table S2**. Properties of the amphiphilic gradient PMeOx-PPhOx copolymers ([PMeOx]:[PPhOx] = 70:30)

| Copolymer | Target DP | $F_{MeOx}$[a] | $M_n$ (kDa)[b] | $Đ$[b] | $D_h$ (nm)[c] | PDI[c] | CMC (mg $L^{-1}$) |
|---|---|---|---|---|---|---|---|
| G1 | 30 | 0.71 | 3.7 | 1.08 | 19.4 | 0.243 | n.d. |
| G2 | 40 | 0.69 | 5.1 | 1.07 | 20.6 | 0.285 | 96 |
| G3 | 60 | 0.70 | 7.4 | 1.10 | 20.1 | 0.056 | 43 |
| G4 | 80 | 0.71 | 9.5 | 1.12 | 24.1 | 0.050 | 23 |
| G5 | 100 | 0.70 | 11.4 | 1.15 | 28.5 | 0.053 | 15 |
| G6 | 120 | 0.71 | 13.2 | 1.20 | 33.8 | 0.032 | 9.2 |
| G7 | 150 | 0.72 | 15.9 | 1.23 | 49.9 | 0.088 | 4.6 |

[a]Fraction of MeOx units in polymer determined by NMR. [b]Determined by SEC. [c]Z-averaged hydrodynamic diameter and dispersity determined by DLS in water ($c_{pol}$=10 mg $L^{-1}$).

**Table S3**. Properties of the amphiphilic block PMeOx-PPhOx copolymers ([PMeOx]:[PPhOx] = 70:30)

| Polymer | Target DP | $F_{MeOx}$[a] | $M_n$ (kDa)[b] | $Đ$[b] | $D_h$ (nm)[c] | PDI[c] | CMC (mg $L^{-1}$) |
|---|---|---|---|---|---|---|---|
| B1 | 30 | 0.70 | 3.8 | 1.09 | 19.3 | 0.479 | n.d. |
| B2 | 40 | 0.72 | 5.2 | 1.08 | 16.6 | 0.088 | 68 |
| B3 | 60 | 0.72 | 7.6 | 1.08 | 19.1 | 0.077 | 32 |
| B4 | 80 | 0.71 | 10.2 | 1.08 | 30.4 | 0.190 | 19 |
| B5 | 100 | 0.70 | 11.9 | 1.13 | 50.6 | 0.281 | 9.6 |
| B6 | 120 | 0.72 | 13.2 | 1.15 | 64.8 | 0.226 | 5.8 |
| B7 | 150 | 0.73 | 16.3 | 1.20 | 82.1 | 0.158 | 3.8 |

[a]Fraction of MeOx units in polymer determined by NMR. [b]Determined by SEC. [c]Z-averaged hydrodynamic diameter and dispersity determined by DLS in water ($c_{pol}$=10 mg $L^{-1}$).

**Table S4**. Properties of the amphiphilic gradient PMeOx-PPhOx copolymers ([PMeOx]:[PPhOx] = 60:40).

| Polymer | Target DP | $F_{MeOx}$[a] | $M_n$ (kDa)[b] | $Đ$[b] | $D_h$ (nm)[c] | PDI[c] | CMC (mg $L^{-1}$) |
|---|---|---|---|---|---|---|---|
| $G1_{60}$ | 30 | 0.62 | 3.8 | 1.09 | 14.4 | 0.089 | n.d. |
| $G2_{60}$ | 40 | 0.61 | 5.0 | 1.10 | 17.4 | 0.039 | 71 |

| | | | | | | | |
|---|---|---|---|---|---|---|---|
| $G3_{60}$ | 60 | 0.60 | 7.6 | 1.09 | 22.4 | 0.024 | n.d. |
| $G4_{60}$ | 80 | 0.62 | 9.8 | 1.10 | 30.7 | 0.065 | n.d. |
| $G5_{60}$ | 100 | 0.61 | 11.6 | 1.14 | 71.5 | 0.158 | 12 |
| $G6_{60}$ | 120 | 0.62 | 13.7 | 1.17 | 123.7 | 0.274 | n.d. |
| $G7_{60}$ | 150 | 0.63 | 16.6 | 1.20 | Insoluble | | |

[a]Fraction of MeOx units in polymer determined by NMR. [b]Determined by SEC. [c]Z-averaged hydrodynamic diameter and dispersity determined by DLS in water ($c_{pol}$=10 mg $L^{-1}$).

**Small-angle neutron scattering (SANS)**

SANS experiments were performed at the Heinz Maier-Leibnitz Zentrum (FRM II reactor, Garching, Germany) on the KWS-2 beamline. Measurements were made on a 128 x 128 multidetector (pixel size 0.8 cm x 0.8 cm) using a non-polarized, monochromatic (wavelength $\lambda$ set by a velocity selector) incident neutron beam collimated with rectangular apertures for two sample-to-detector distances, namely 2 and 8 m (with $\lambda$ = 0.6 nm). With this setup, the investigated $q$-range was 0.06 $nm^{-1}$ to 3 $nm^{-1}$. In all cases, the two-dimensional scattering patterns were isotropic and were azimuthally averaged, resulting in the dependence of the scattered intensity $I_s(q)$ on $q$. The curves were corrected for background scattering and detector efficiency. The intensities of neutron scattering are given in absolute units, $cm^{-1}$. All polymers were used as is without deuteration and dissolved either in $D_2O$ or $D_2O/H_2O$ mixtures. The concentration of all samples was set to 5 mg/ml and the measurements were performed at 25°C.

*SANS data fitting*

The scattering length densities of the micelle components are shown in Table SANS SI-1.

The scattered intensity curves were fitted using the model of block copolymer ellipsoidal micelle implemented in SASFit software[1] based on the model developed by Pedersen et al.[2] The scattering curves in $D_2O$ could be fitted using the following function:

$$I(q) = P_{sgc}(q)S(q)$$

(SANS 1)

We assume that $S(q) = 1$ due to low concentration of nanoparticles in solution, 5 mg/mL. The overall scattering intensity of the block copolymer ellipsoidal micelle written as:

$$P_{sgc} = N_{agg}^2\beta_{core}^2P_{core}(q) + N_{agg}\beta_{brush}^2P_{brush}(q) + 2N_{agg}^2\beta_{core}\beta_{brush}S_{brush-core}(q) + N_{agg}(N_{agg}-1)\beta_{brush}^2S_{brush-brush}(q)$$

(SANS 2)

where $N_{agg}^2\beta_{core}^2P_{core}(q)$ is the self-correlation term of the core; $N_{agg}\beta_{brush}^2P_{brush}(q)$ is the self-correlation term of the chains; $2N_{agg}^2\beta_{core}\beta_{brush}S_{brush-core}(q)$ is the cross-term between the core and chains and $N_{agg}(N_{agg}-1)\beta_{brush}^2S_{brush-brush}(q)$ is the cross-term between different chains. $N_{agg}$ is the aggregation number of polymers forming the nanoparticle per surface area, $\beta_{brush}=V_{brush}(\eta_{brush}-\eta_{solv})$ and $\beta_{core}=V_{core}(\eta_{core}-\eta_{solv})$ are the excess scattering lengths of a block in the corona and in the core, respectively. $V_{brush}$ and $V_{core}$ are the total volume of a block in the corona and in the core, respectively. $\eta_{brush}$ and $\eta_{core}$ are the corresponding scattering length densities (SLDs). $P_{core}(q)$ is scattering of spherical core

$$P_{core}(q,R_{core})=3\frac{(\sin(qR_{core})-qR_{core}cos(qR_{core}))}{(qR_{core})^3}$$

(SANS 3)

The scattering intensity for the brush is given by:

$$P_{brush}(q,R_{gchain})=2\frac{exp(-x)-1+x}{x^2}$$

(SANS 4)

where $x=R_{gchain}^2q^2$; $R_{gchain}$ is the gyration radius of a polymer chain.

The contribution of the cross term between core and chains which form a brush of worm-like micelle is calculated using the equation:

$$S_{brush-core}(q,R_{core},R_{gchain},d)=\psi(qR_{gchain})P_{core}(q,R_{core})\frac{sin(q[R_{core}+dR_{gchain}])}{q[R_{core}+dR_{gchain}]}$$

(SANS 5)

where $\psi(qR_{gchain})=\frac{1-exp(-x)}{x}$ is the form factor amplitude of the chain.

The contribution of the cross term between chains is calculated using the equation:

$$S_{brush-brush}(q,R_{core},R_{gchain},d)=\psi^2(qR_{gchain})\left[\frac{sin(q[R_{core}+dR_{gchain}])}{q[R_{core}+dR_{gchain}]}\right]^2$$

(SANS 6)

where $d$ is the parameter that accounts for non-penetration of the chains into the core and should be mimicked by $d\sim1$ for $R_{core}$"$R_{gchain}$.

The model has the following fitting parameters: $N_{agg}$ – aggregation number; $V_{core}$ – molecular volume of single block unit in the micellar core; $V_{brush}$ – molecular volume of single block unit in the micellar corona; $\eta_{core}$ – scattering length density of spherical core; $\eta_{brush}$ – scattering length density of the block unit in the corona; $\eta_{solv}$ – scattering length density of solvent; $R_{gchain}$ – gyration radius of polymer chains in the corona.

Excess scattering lengths of solvent and polymeric shell, $V_{core}$, $V_{brush}$, were known from literature data and polymer composition and were chosen to be fixed during the fitting procedure.

To account for nanoparticles polydispersity, a Schulz-Zimm distribution of $N_{agg}$ with polydispersity parameter $\sigma$ was included in the following way:

$$SZ = \frac{Nagg}{\Gamma(Z+1)}\left(\frac{Z+1}{<Nagg>}\right)^{Z+1} exp\left[-\frac{(Z+1)Nagg}{<Nagg>}\right]$$

(SANS 7)

where $Z = \frac{1}{\sigma^2} - 1$

(SANS 8)

The gyration radius $R_g$ of nanoparticles was calculated from the Guinier regime to evaluate the overall size of nanoparticles.

**Cryo-TEM**

Samples were analyzed by cryogenic transmission electron microscopy (cryo-TEM) following the previous description.[3] Initially, samples were equilibrated at 25 °C at high relative humidity (> 90%) within a climate chamber. A small drop (< 1 µl) of each sample was deposited on a carbon-sputtered copper grid covered with a perforated polymer film. Excess liquid was removed by blotting with a filter paper, leaving a thin film of the solution on the grid. Subsequently, the sample was vitrified in liquid ethane and transferred to the microscope. Samples were kept below –160°C and protected against atmospheric conditions during both transfer and examination. Analyses were performed with a Zeiss Libra 120 Transmission Electron Microscope (Carl Zeiss AG, Oberkochen, Germany) operating at 80kV and in zero-loss bright-field mode. Digital images were recorded under low-dose conditions with a BioVision Pro-SM Slow Scan CCD camera (Proscan Elektronische Systeme GmbH, Scheuring, Germany).

**Determination of critical micelle concentration (cmc)**

Solutions of the copolymers were prepared by direct dissolution in phosphate-buffered saline (PBS, 150 mM, pH 7.4) at a concentration of 1 mg $mL^{-1}$ and were successively diluted to a concentration of $10^{-5}$ mg $mL^{-1}$. A pyrene stock solution ($1.2 \times 10^{-4}$ mol $L^{-1}$ in acetone) was added to each polymer sample to obtain a final concentration of pyrene in PBS of 6 $10^{-7}$ mol $L^{-1}$. Fluorescence spectra of the samples were recorded with a Cary Eclipse spectrophotometer (under stirring) equipped with a Varian Cary Temperature Controller, equilibrated for 10 min

at 37 °C, using excitation at 333 nm. The ratio of the fluorescence emission intensities at 373 nm ($I_1$) and at 384 ($I_3$) were plotted against the polymer concentration. The cmc was determined as the intersection between the plateau at $d(I_1/I_3)/dc \approx 0$ and the tangent of the curve where the $I_1/I_3$ ratio decreased with an increasing copolymer concentration.

**Förster resonance energy transfer (FRET) spectroscopy**

First piperazine end-capped G5 and B5 copolymers were synthesized according to the abovementioned general procedure, whereby the polymerizations were terminated with a five-fold excess of piperazine in anhydrous methanol (1M) followed by precipitation in cold diethyl ether, filtration and drying under vacuum. These polymers (100 mg) were then dissolved in *N,N*-dimethylacetamide (5 mL) together with FITC (1.2 eq.) or RITC (1.2 eq) and triethylamine (2 eq.). The mixture was vortexed at room temperature overnight, followed by removal of unreacted dye using Sephadex LH-20 column in methanol. The polymer containing fractions were evaporated under reduced pressure, dissolved in distilled water and freeze-dried.

The dynamic stability of the micelles was studied by FRET exchange experiments. Therefore, stock solutions of mixed micelles containing 9.8 mg/mL of the unlabeled copolymer (e.g., G5) and 0.2 mg/mL of the fluorescently labeled copolymer (e.g., G5-FITC or G5-RITC) of the same type were prepared by dissolution in PBS and were allowed to equilibrate at RT overnight. Afterward, 100 uL of the FITC labeled, respectively RITC labeled copolymer were mixed with 1.8 mL of PBS and the fluorescence emission of the sample at 575 nm (excitation 460 nm) was measured immediately to obtain $I_0$. The samples were then left for equilibration in the thermostatted Peltier cell (25 °C) of the fluorescence spectrometer, recording the emission at 575 nm ($I_t$) every 2 min. The emission intensity time-dependence data was fitted with a double-exponential equation

$$I_t = a_1(e^{-k_1 t}) + a_2(e^{-k_2 t}) + I_0$$

where $I_t$ accounts for the emission intensity at time t, $k_1$and $k_2$ being the rate constants, $a_1$ and $a_2$ the corresponding amplitudes, $y_0$ the emission intensity offset. To visualize the difference between the copolymers, the emission intensities were normalized to the 0 - 100% scale, where 0% is $I_0$ and 100% represents $\lim_{t\to\infty} I_t$ value. All measurements were performed in triplicates with independently prepared micelle samples.

**Drug loading**

*Thin-film rehydration method*

The stock solution of the copolymer (500 uL, 20 mg $mL^{-1}$ in ethanol) and curcumin (200 uL, 400 uL or 600 uL, 5 mg $mL^{-1}$ in ethanol) were mixed in the desired ratio in 2 mL Eppendorf tube, dried at 55 °C in a stream of air, followed by drying at high vacuum overnight. Preheated PBS solution (1 mL, pH 7.4, 150 mM, 55 °C) was added to each tube, followed by vortexing for 1 h. Insoluble curcumin was removed by centrifugation (10 000 rpm). 50 uL was taken for UV-Vis spectroscopy (diluted with 950 uL ethanol (diluted 10x with ethanol if necessary)), 200 uL for DLS (diluted with 800 uL PBS) and 600 uL for picture and stability. The supernatant was filtered through a 0.22 μm syringe filter. The amount of loaded curcumin was determined by UV-Vis spectroscopy in ethanol at 424 nm using curcumin calibration. Then, the drug loading was calculated as $DL = m_{cur} / (m_{pol} + m_{cur}) \times 100\ \%$, where $m_{cur}$ and $m_{MB4}$ are the weight amounts of the solubilized curcumin and copolymer in the dispersion and the loading efficiency $LE = m_{cur} / m_{cur\ added} \times 100\ \%$, where $m_{cur\ added}$ is the initial amount of curcumin added to the polymer solution. Each loading experiment was performed in triplicate.

*Direct dissolution*

Solid curcumin (12 mg) was dispersed in 1 mL of the copolymer solution in PBS (10 mg $mL^{-1}$) and incubated at 65 °C for 72 h with an occasional vortex. The solution gradually changed color to dark brown. Insoluble curcumin was removed by centrifugation (10 000 rpm). Samples of nanoformulations were further analyzed as mentioned above: 50 uL was taken for UV-Vis spectroscopic analysis (diluted with 950 uL ethanol, further diluted with ethanol if necessary)), 200 uL for DLS (diluted with 800 uL PBS) and 600 uL for stability assay. Each loading experiment was performed in triplicate.

*DMSO-assisted direct dissolution*

The polymer was dissolved in PBS (10 mg $mL^{-1}$) and equilibrated at RT for 1 h. The concentrated stock solution of curcumin in DMSO (100 mg $mL^{-1}$) was added and the mixture was vigorously vortexed for 15 min. The maximal amount of DMSO in nanoformulations was 3% (v/v). Insoluble (if any) curcumin was removed by centrifugation (10 000 rpm). The formulations were analyzed by UV-VIS spectroscopy and DLS as described above. Each loading experiment was performed in triplicate.

*Nanoprecipitation*

The solution of curcumin (10 mg) and copolymer (10 mg) in ethanol (5 mL) was injected into the rapidly stirred solution of PBS (5 mL). After equilibration at 40 °C for 3 h, the volume of the nanoformulation solution was reduced to 3.5 mL using rotary evaporation, followed by adding 1.5 mL of distilled water. Insoluble curcumin was removed by centrifugation (10 000

rpm) and the nanoformulations were analyzed as described above. Each loading experiment was performed in triplicate.

**Spectroscopic studies of the curcumin-loaded micelles**

In all the measurements, the concentration of the curcumin-loaded micelles was 50 mg $L^{-1}$. UV-Vis absorption spectra were recorded using a Shimadzu UV-2501PC (Shimadzu, Japan) spectrophotometer. Steady-state fluorescence and phosphorescence spectra were recorded with an FLS-1000 (Edinburgh Instruments, UK) spectrofluorometer equipped with double excitation and emission monochromators. Time-resolved fluorescence was measured using a time-correlated single-photon counting (TCSPC) system (Pico-Quant GmBH, Chaussee, Germany) consisting of a PicoHarp 300 controller and a PDL 800-B driver. The samples were excited with the pulsed diode laser head LDH-P-C-405 at 405 nm at a time resolution of 64 ps. The signals were detected with a microchannel plate photomultiplier tube (Hamamatsu R2809U). The influence of the scattered excitation light was reduced with a cutoff filter (transmission > 420 nm) in front of the monitoring monochromator. Fluorescence decays were collected at 620 nm. The instrumental response function (IRF) was measured separately, and the decays were deconvoluted and fitted by applying the iterative least-squares method to the sum of 3 exponents (eq FLIM1)

$$I(t) = \sum_i a_i e^{-t/\tau_i} \quad \text{(FLIM 1)}$$

In this equation, $\tau_i$ is the fluorescence lifetime and $a_i$ is the amplitude (pre-exponential factor) of each decay component. The mean amplitude weighted lifetime $\langle\tau\rangle$ was calculated using eq FLIM2:

$$< \tau > = \frac{\sum a_i \tau_i}{\sum a_i} \quad \text{(FLIM 2)}$$

**Stability of the formulations**

The formulations prepared by direct dissolution method ($c_{pol}$ = 10 mg $mL^{-1}$, $c_{cur,0}$ = 2 mg $mL^{-1}$) were freeze-dried to remove water. Afterward, the dry samples were re-dissolved in distilled water, centrifuged (10 000 rpm) to remove insoluble curcumin (if any) and analyzed by DLS and UV-VIS spectroscopy.

**Curcumin release**

The curcumin release experiments were performed at 37 °C in a buffered medium (PBS, pH 7.4). Aliquots of the formulations prepared by direct dissolution method (2 mL, $c_{pol}$ = 10 mg $mL^{-1}$, $c_{cur,0}$ = 2 mg, three independently prepared formulations per copolymer) were loaded into the dialysis tubings (MWCO = 50 kDa) and dialyzed against 5 L of PBS (pH 7.4, 150 mM) at

37°C. The buffer was replaced frequently due to the low equilibrium solubility of free curcumin. At predetermined time points, 50 uL of the micellar solution was removed from the dialysis system and 50 uL was taken for curcumin content analysis by UV-VIS. No macroscopic precipitation was observed during the dialysis experiment. The experiment was performed in duplicates with three independently prepared formulations per copolymer (n = 6).

**Cell cultures**

Human breast cancer MDA-MB-231 cells are cultured with DMEM (Lonza)-containing 10% FBS (Gibco). Human normal breast cells MCF-10A were cultured in DMEM/F12 medium (Gibco) containing 5% FBS (Gibco), Glucose (Sigma, 4,5g/L), human insulin, (Sigma, 10μg/mL), hydrocortisone (Sigma, 0.5μg/mL), cholera toxin (Sigma, 0.1μg/mL), epidermal growth factor EGF (Peprotech, 20ng/mL) and 2 mM L-glutamine (Gibco), in a humidified incubator with 5% CO2. MCF-10A cells are kindly provided by Prof. Jukka Westermarck (Turku Bioscience Centre, Turku, Finland).

**Cytotoxicity assay**

The efficacy of the free curcumin and curcumin-loaded B5Cur and G5Cur polymers in cancer cells and normal cells was determined by the WST-1 cell viability assay. MDA-MB-231 cancer cells and MCF-10A cells were placed in a 96-well plate (2000 cells per well, three parallel wells for each concentration) in a complete growth medium with 5% FBS at 37 ° C, 5% $CO_2$ overnight. Then, the medium was replaced with a fresh medium containing curcumin or curcumin-loaded polymers at indicated concentrations for 48 hours. The curcumin-loaded B5Cur and G5Cur micelles were prepared in water and cell medium. The stock solution of free curcumin was dissolved in absolute ethanol, followed by a high dilution with cell medium into working concentration. For WST-1 assay, 10 μL of WST-1 reagent (Roche) dissolving in 100 μL complete growth medium to replace the drug-contained medium for each well. After incubated in a cell incubator for 2 hours, the absorbance was measured at 440 nm with a Varioskan™ LUX Multimode Reader (Thermo Scientific Inc., Waltham, MA, USA).

**Statistical analyses**

All data are presented as the means ± standard deviations (SD). Statistical graphs were generated using GraphPad Prism 8 software (GraphPad Software, Inc., San Diego, CA). The statistical significance of differences between the two groups was determined by two-way ANOVA analysis. *$p < 0.05$ was considered statistically significant.

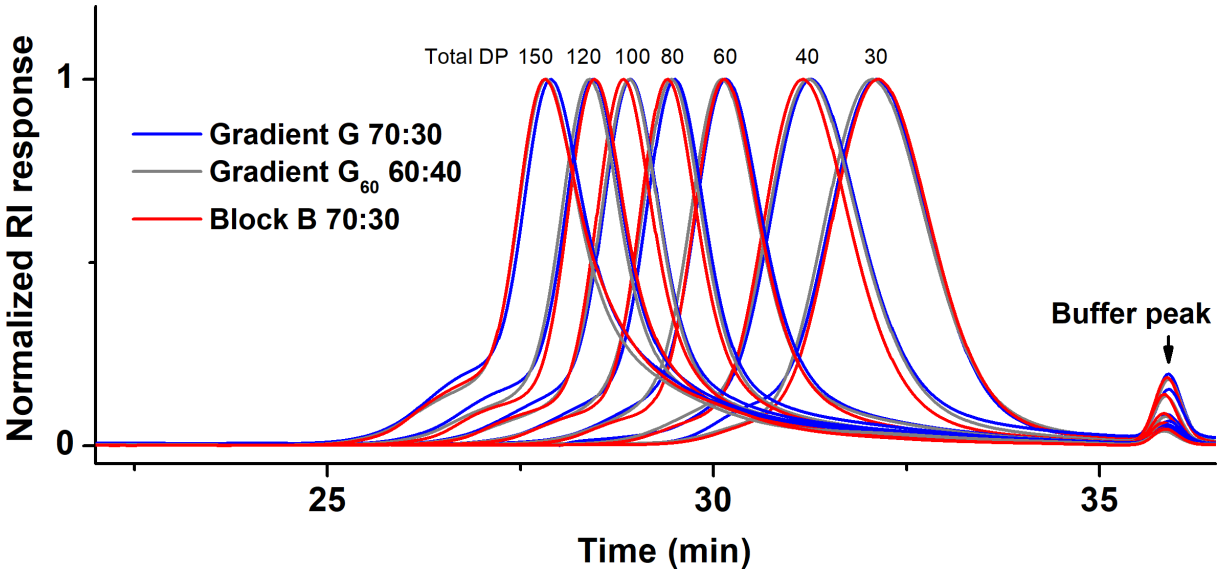


**Figure S1.** SEC traces of all synthesized PMeOx-PPhOx copolymers eluted with DMA-LiCl.

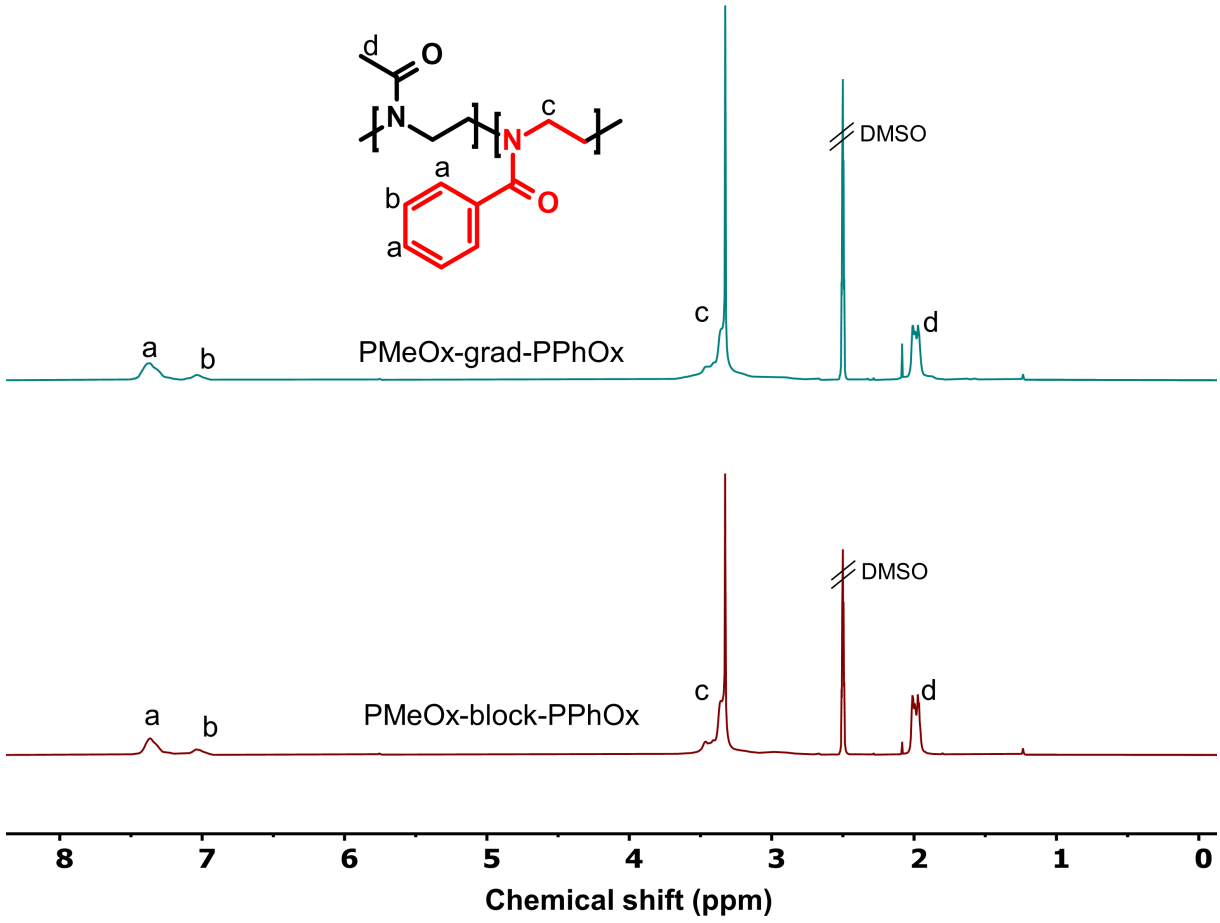


**Figure S2.** $^{1}$H NMR spectra of copolymers G7 (top), B7(bottom) DMSO-$d_6$.

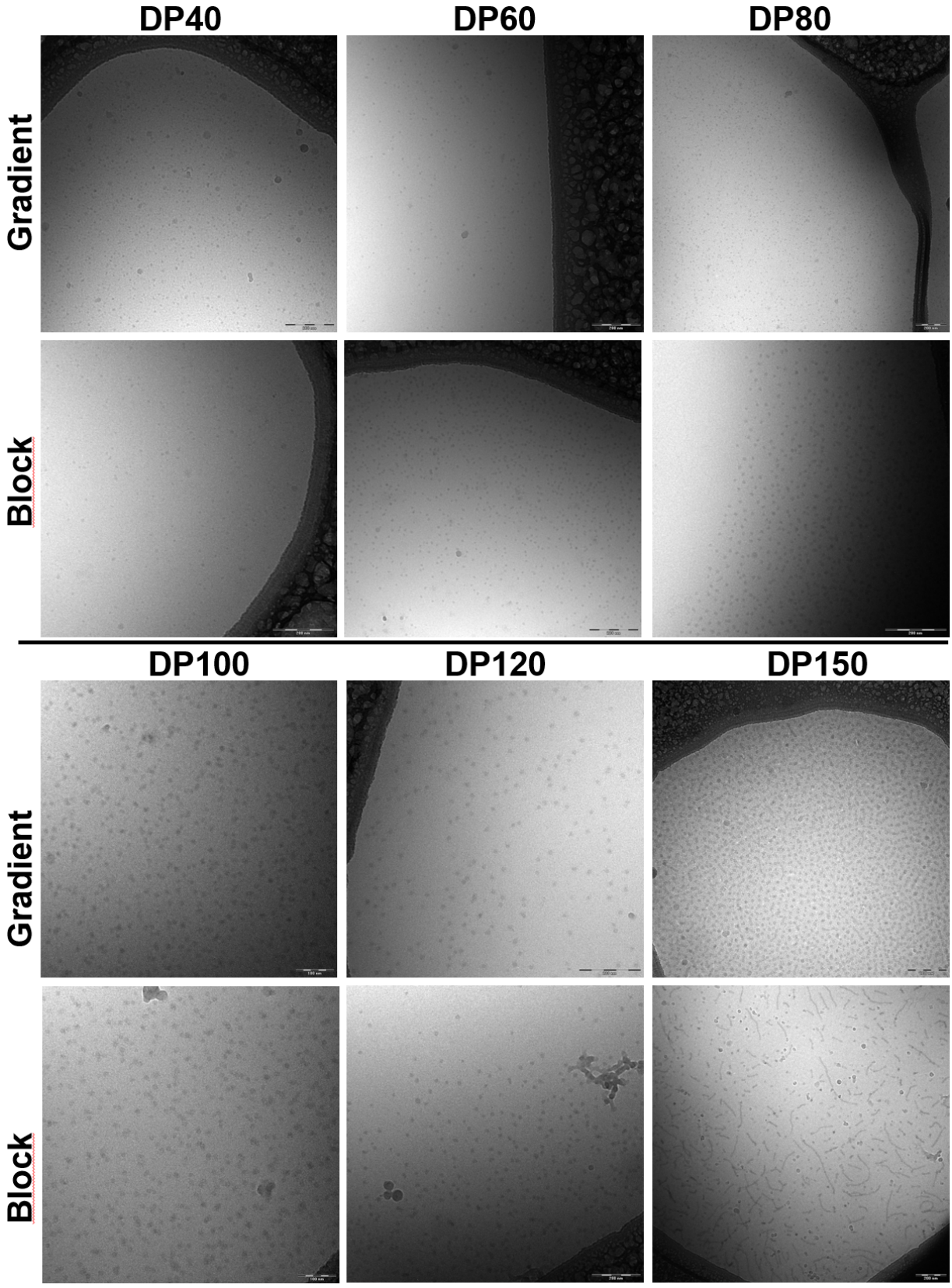


**Figure S3.** CryoTEM images of G2-7, respectively B2-7 nanoparticles in water. The scale bars represent 200 nm.

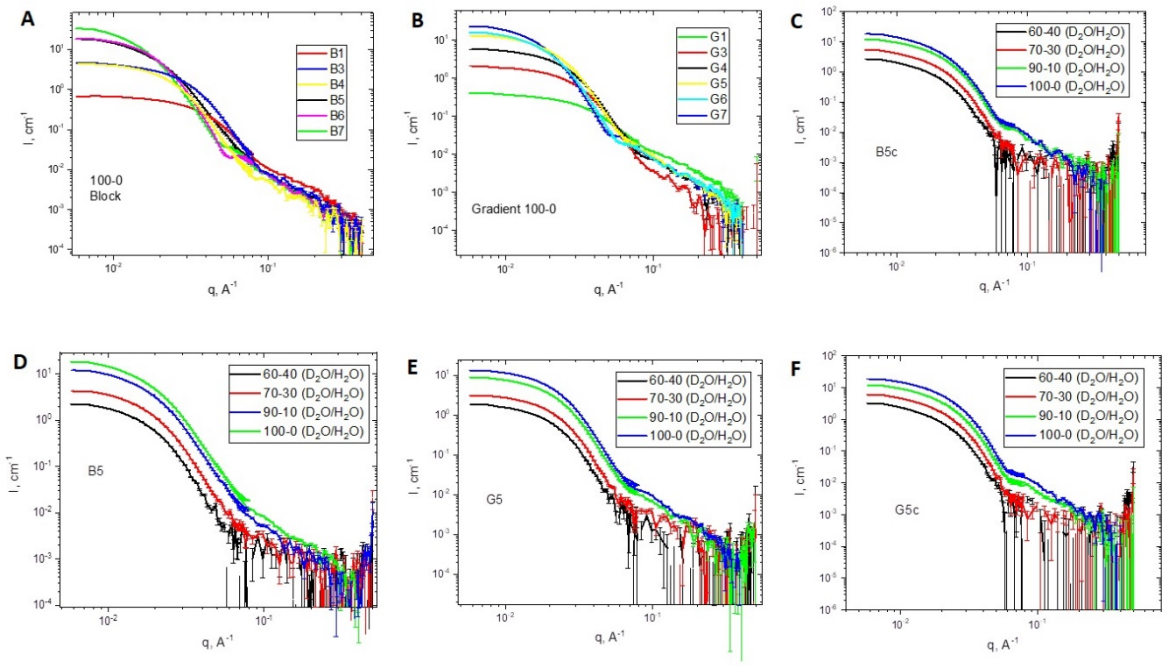


**Figure S4.** SANS curves of copolymers in water at 25 °C. SANS curves of block copolymers in $D_2O$ (A). SANS curves of gradient copolymers in $D_2O$ (B). SANS curves of B5Cur copolymer in the mixture $D_2O/H_2O$ (C). SANS curves of B5 copolymer in the mixture $D_2O/H_2O$ (D). SANS curves of G5 copolymer in the mixture $D_2O/H_2O$ (E). SANS curves of G5Cur copolymer in the mixture $D_2O/H_2O$ (F).

**Table S4.** Fitting results of SANS data for copolymers in $D_2O$.

| Sample | DP | $N_{aggr}$ | σ | $R_g$, A | ε |
|---|---|---|---|---|---|
| B1 | 30 | 35 | 0.11 | 15 | 1.1 |
| B3 | 60 | 78 | 0.58 | 19 | 1.1 |
| B4 | 80 | 97 | 0.5 | 27 | 1.5 |
| B5 | 100 | 197 | 0.82 | 31 | 1.6 |
| B6 | 120 | 220 | 0.41 | 40 | 1.2 |
| B7 | 150 | 297 | 0.56 | 51 | 1.5 |
| | | | | | |
| G1 | 30 | 27 | 0.07 | 16 | 1.1 |
| G3 | 60 | 76 | 0.6 | 22 | 1.1 |
| G4 | 80 | 101 | 0.67 | 27 | 1.5 |

| | | | | | |
|---|---|---|---|---|---|
| G5 | 100 | 133 | 0.57 | 33 | 1.4 |
| G6 | 120 | 169 | 0.46 | 39 | 1.2 |
| G7 | 150 | 231 | 0.49 | 43 | 1.3 |
| | | | | | |
| B5Cur | 100 | 137 | 0.45 | 52 | 1.4 |
| G5Cur | 100 | 158 | 0.27 | 50 | 1.3 |

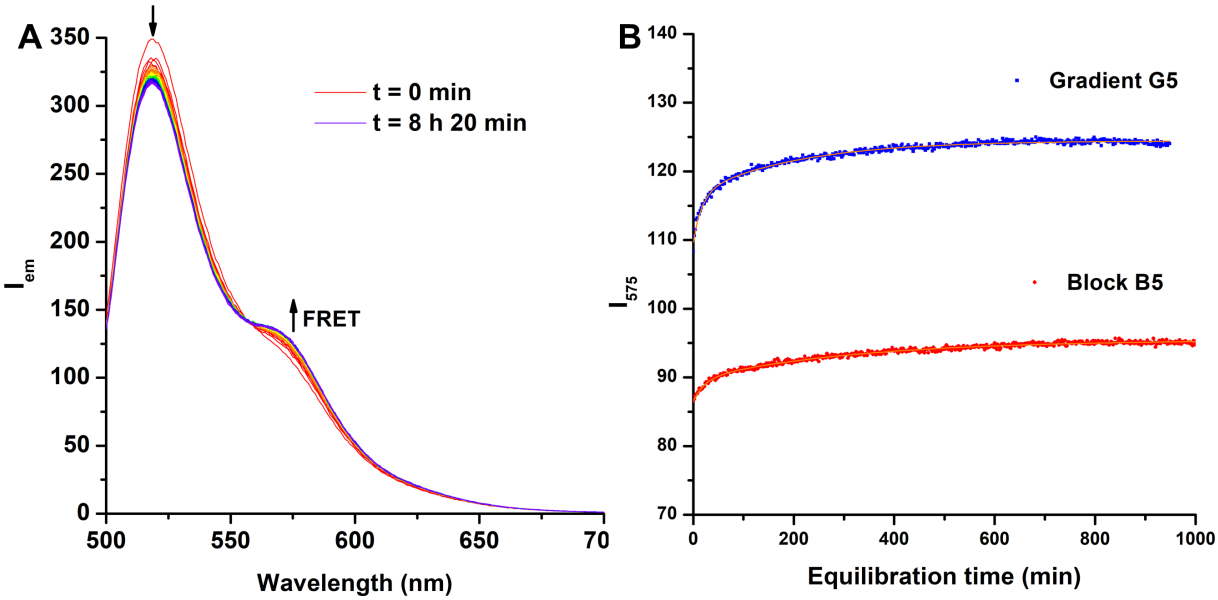


**Figure S5.** Measurement of the monomer exchange kinetics by time-resolved Förster resonance energy transfer (FRET) spectroscopy of fluorescently labeled micelles ($c_{pol}$ = 1 mg mL$^{-1}$) in PBS (pH = 7.4) at 25°C. (A) Fluorescence emission spectra of G5 micelles ($\lambda_{ex}$ = 455 nm) were measured at increasing equilibration time (step 10 min). (B) The fluorescence emission intensity of G5, respectively B5, micelles at 575 nm ($\lambda_{ex}$ = 455 nm) measured at increasing equilibration time (step 2 min). (B)

**Table S5.** Unimer exchange kinetics measured by FRET at 25 °C.

| Polymer | $k_1$ ($10^{-5}$ s$^{-1}$) | $t_{1/2,1}$ (min) | $k_2$ ($10^{-5}$ s$^{-1}$) | $t_{1/2,2}$ (min) |
|---|---|---|---|---|
| G5 | 104.4 ± 6.4 | 11.1 ±0.7 | 7.9 ± 0.5 | 145.8 ± 8.7 |
| B5 | 71.9 ± 0.9 | 16.1 ±0.2 | 5.3 ± 0.2 | 218.2 ± 6.9 |

**Table S6**. Achieved curcumin concentrations, loading efficiencies (LE) and drug loadings (DL) in PBS (pH = 7.4) solubilized by different copolymers using the thin film hydration technique. Polymer concentration 10 mg $mL^{-1}$, differing in the curcumin feed.

| Polymer | Curcumin feed (mg $mL^{-1}$) | Solubilized curcumin (mg $mL^{-1}$) | LE (%) | DL (%) |
|---|---|---|---|---|
| G2 | 1 | 0.80 ± 0.02 | 80.1 ± 2.5 | 7.4 ± 0.2 |
| | 2 | 1.66 ± 0.06 | 82.8 ± 4.7 | 14.2 ± 0.9 |
| | 4 | 0.75 ± 0.07 | 18.7 ± 3.6 | 7.0 ± 1.4 |
| B2 | 1 | 0.89 ± 0.03 | 89.3 ± 3.3 | 8.2 ± 0.3 |
| | 2 | 1.94 ± 0.05 | 96.8 ± 2.3 | 16.2 ± 0.5 |
| | 4 | 1.76 ± 0.07 | 44.0 ± 1.8 | 15.0 ± 0.7 |
| G3 | 1 | 0.82 ± 0.04 | 81.7 ± 4.1 | 7.6 ± 0.4 |
| | 2 | 1.37 ± 0.07 | 68.7 ± 3.6 | 12.1 ± 0.7 |
| | 4 | 0.03 ± 0.01 | 0.8 ± 0.1 | 0.3 ± 0.1 |
| B3 | 1 | 0.97 ± 0.01 | 96.7 ± 1.3 | 8.8 ± 0.1 |
| | 2 | 1.94 ± 0.02 | 97.0 ± 1.1 | 16.2 ± 0.2 |
| | 4 | 1.31 ± 0.04 | 32.7 ± 1.0 | 11.6 ± 0.4 |
| G4 | 1 | 0.83 ± 0.04 | 83.2 ± 3.9 | 7.7 ± 0.4 |
| | 2 | 0.06 ± 0.10 | 3.0 ± 4.9 | 0.6 ± 1.0 |
| | 4 | n.d. | n.d. | n.d. |
| B4 | 1 | 0.99 ± 0.01 | 98.6 ± 0.9 | 9.0 ± 0.1 |
| | 2 | 1.90 ± 0.04 | 94.8 ± 1.8 | 15.9 ± 0.4 |
| | 4 | 0.42 ± 0.28 | 10.5 ± 7.0 | 4.0 ± 2.7 |
| G5 | 1 | 0.19 ± 0.11 | 19.4 ± 11.3 | 1.9 ± 1.1 |
| | 2 | n.d. | n.d. | n.d. |
| | 4 | n.d. | n.d. | n.d. |
| B5 | 1 | 0.97 ± 0.03 | 97.1 ± 3.0 | 8.8 ± 0.3 |
| | 2 | 1.55 ± 0.07 | 77.6 ± 3.4 | 13.4 ± 0.7 |
| | 4 | 0.07 ± 0.01 | 1.7 ± 0.4 | 0.7 ± 0.1 |
| G6 | 1 | 0.09 ± 0.01 | 9.0 ± 0.7 | 0.9 ± 0.1 |
| | 2 | n.d. | n.d. | n.d. |

| | | | | |
|---|---|---|---|---|
| | 4 | n.d. | n.d. | n.d. |
| B6 | 1 | 0.97 ± 0.05 | 96.5 ± 4.5 | 8.8 ± 0.5 |
| | 2 | 0.55 ± 0.08 | 27.7 ± 4.2 | 5.3 ± 0.8 |
| | 4 | 0.02 ± 0.01 | 0.5 ± 0.3 | 0.2 ± 0.1 |
| G7 | 1 | 0.03 ± 0.02 | 2.8 ± 1.8 | 0.3 ± 0.2 |
| | 2 | n.d. | n.d. | n.d. |
| | 4 | n.d. | n.d. | n.d. |
| B7 | 1 | 0.46 ± 0.08 | 46.2 ± 8.0 | 4.4 ± 0.8 |
| | 2 | 0.07 ± 0.03 | 3.5 ± 1.6 | 0.7 ± 0.3 |
| | 4 | n.d. | n.d. | n.d. |

**Table S7**. Achieved curcumin concentrations, loading efficiencies (LE) and drug loadings (DL) in PBS (pH = 7.4) solubilized by different copolymers via direct dissolution of solid curcumin. Polymer concentration 10 mg $mL^{-1}$, curcumin feed 12 mg $mL^{-1}$.

| Polymer | Solubilized curcumin (mg $mL^{-1}$) | LE (%) | DL (%) |
|---|---|---|---|
| G2 | 1.32 ± 0.01 | 13.2 ± 0.1 | 11.7 ± 0.1 |
| B2 | 1.34 ± 0.003 | 13.4 ± 0.03 | 11.8 ± 0.02 |
| G3 | 1.84 ± 0.02 | 18.4 ± 0.2 | 15.6 ± 0.1 |
| B3 | 1.75 ± 0.07 | 17.5 ± 0.7 | 14.9 ± 0.5 |
| G4 | 1.67 ± 0.13 | 16.7 ± 1.3 | 14.3 ± 0.9 |
| B4 | 1.62 ± 0.07 | 16.2 ± 0.7 | 13.9 ± 0.5 |
| G5 | 1.77 ± 0.05 | 17.7 ± 0.5 | 15.0 ± 0.4 |
| B5 | 1.74 ± 0.03 | 17.4 ± 0.3 | 14.8 ± 0.2 |
| G6 | 1.65 ± 0.02 | 16.5 ± 0.2 | 14.2 ± 0.1 |
| B6 | 1.63 ± 0.32 | 16.3 ± 3.2 | 14.0 ± 2.4 |
| G7 | 1.72 ± 0.17 | 17.2 ± 1.7 | 14.7 ± 1.2 |
| B7 | 1.72 ± 0.09 | 17.2 ± 0.9 | 14.7 ± 0.6 |

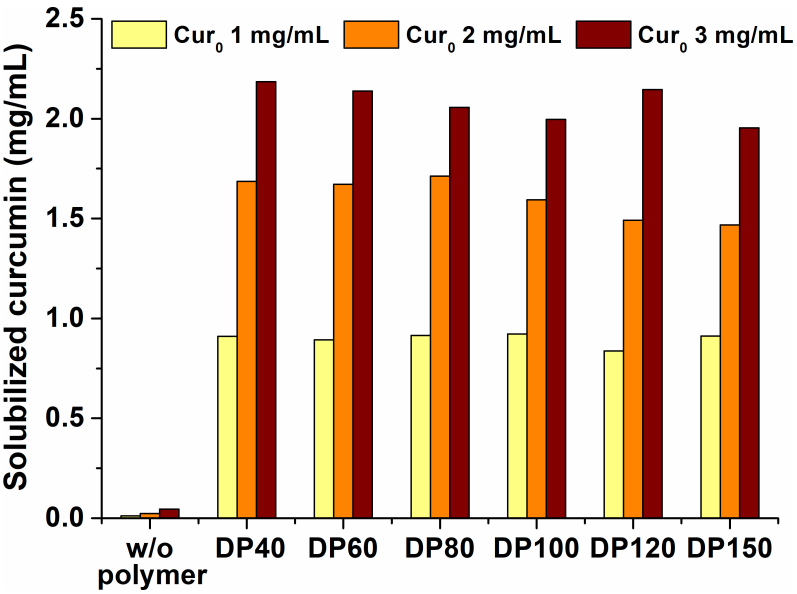


**Figure S6.** Achieved concentrations of curcumin solubilized by gradient copolymers G2-7 by addition of different amounts of concentrated curcumin solution in DMSO (100 mg $mL^{-1}$) into the polymer solution in PBS ($c_{pol}$ = 10 mg $mL^{-1}$) or a buffer without any polymer.

**Table S8.** Achieved curcumin concentrations, loading efficiencies and drug loadings in PBS (pH = 7.4) solubilized by different copolymers using the nanoprecipitation technique. Polymer concentration 2 mg $mL^{-1}$, curcumin feed 2 mg $mL^{-1}$.

| Polymer | Solubilized curcumin (mg $mL^{-1}$) | LE (%) | DL (%) |
|---|---|---|---|
| G2 | 0.39 ± 0.01 | 19.3 ± 0.6 | 16.1 ± 0.5 |
| B2 | 0.39 ± 0.02 | 19.6 ± 1.0 | 16.4 ±0.9 |
| G5 | 0.40 ± 0.02 | 20.0 ± 1.2 | 16.7 ± 1.1 |
| B5 | 0.39 ± 0.01 | 16.9 ± 0.7 | 16.5 ± 0.7 |
| G7 | 0.40 ± 0.02 | 20.1 ± 0.8 | 16.7 ± 0.8 |
| B7 | 0.41 ± 0.03 | 20.4 ±1.3 | 16.9 ± 1.3 |

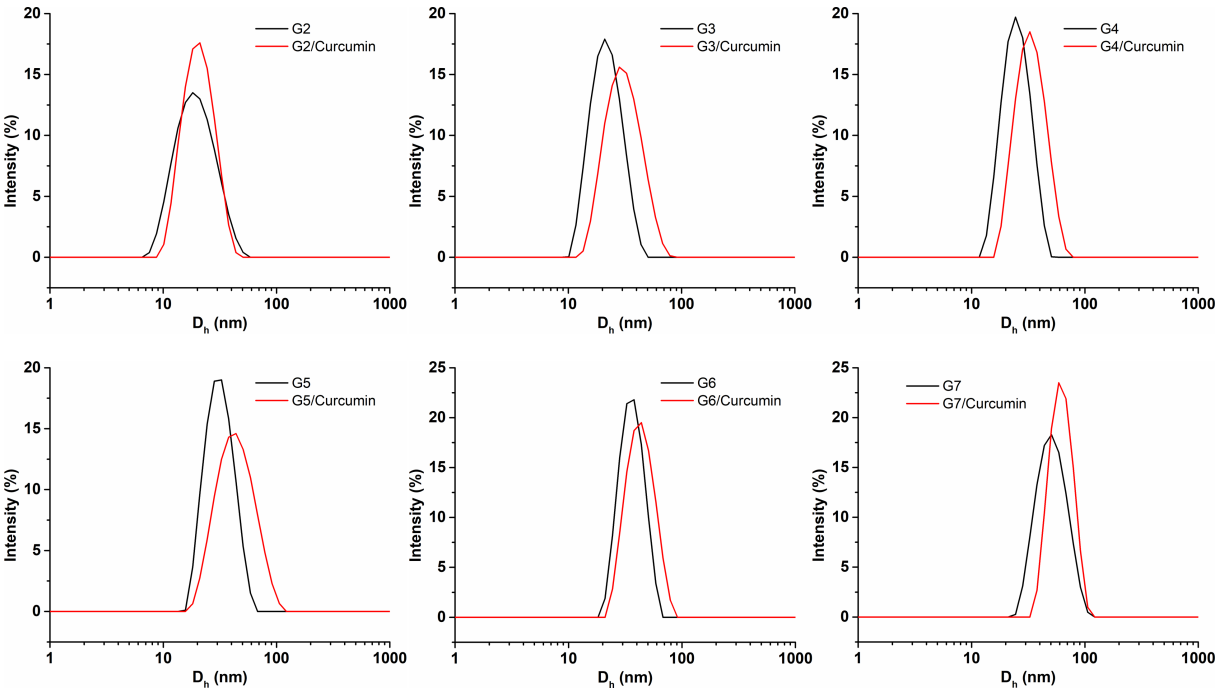


**Figure S7**. Size of the nanoparticles before and after the direct incapsulation of solid curcumin (Table S7) by different copolymers, diluted to $c_{pol}$ = 2 mg $mL^{-1}$ in PBS (pH = 7.4, 25 °C).

**Table S9**. Size of the nanoparticle before and after the direct incapsulation of solid curcumin (Table S7) by different copolymers, diluted to $c_{pol}$ = 2 mg $mL^{-1}$ in PBS (pH = 7.4, 25 °C).

| Polymer | Curcumin-free micelles | | Curcumin-loaded micelles | |
|---|---|---|---|---|
| | $D_h$ (nm) | PDI | $D_h$ (nm) | PDI |
| G2 | 19.78 | 0.24 | 19.44 | 0.07 |
| B2 | 18.82 | 0.24 | 19.02 | 0.11 |
| G3 | 20.24 | 0.07 | 28.94 | 0.13 |
| B3 | 24.09 | 0.15 | 29.12 | 0.15 |
| G4 | 24.16 | 0.07 | 31.09 | 0.08 |
| B4 | 27.23 | 0.04 | 30.6 | 0.06 |
| G5 | 29.53 | 0.08 | 39.97 | 0.13 |
| B5 | 36.01 | 0.20 | 41.97 | 0.13 |
| G6 | 34.83 | 0.03 | 40.61 | 0.06 |
| B6 | 37.41 | 0.04 | 50.97 | 0.04 |
| G7 | 48.44 | 0.07 | 56.56 | 0.03 |
| B7 | 57.98 | 0.02 | 63.2 | 0.04 |

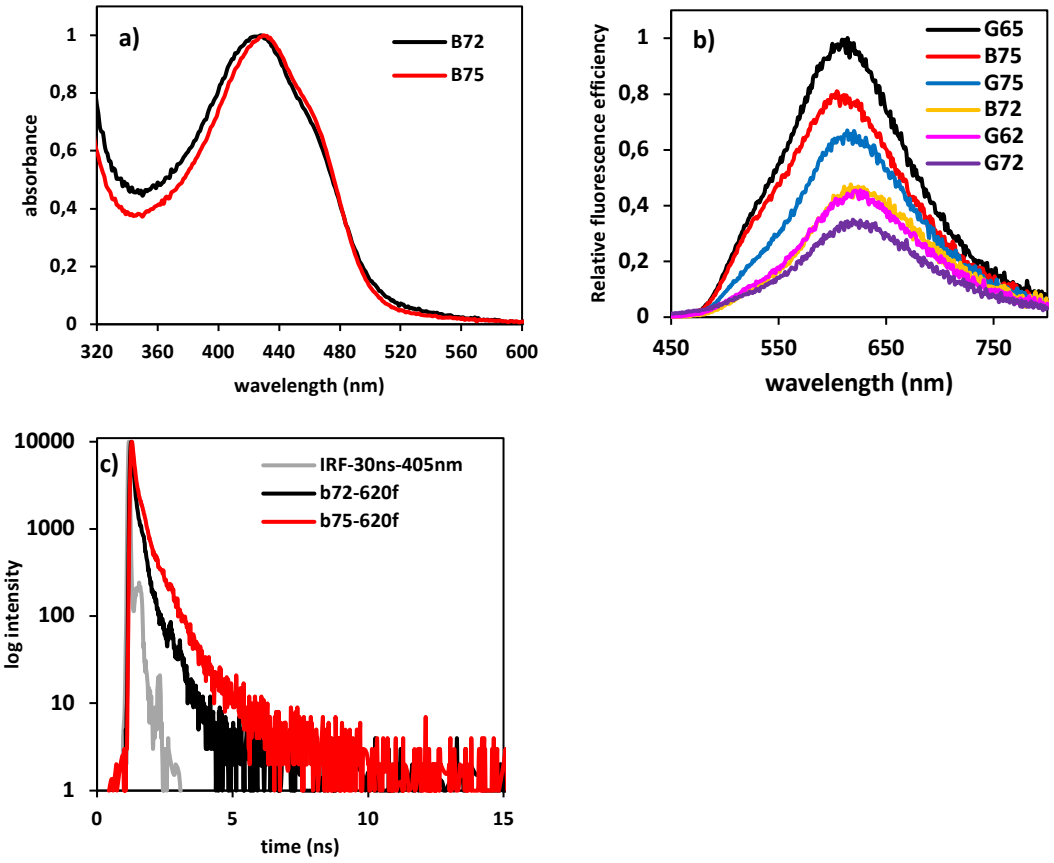


**Figure S8.** A) Normalized absorption spectra, B) fluorescence spectra and fluorescence decay curves of selected formulations. For both fluorescence spectra and decay curves, the excitation wavelength was 405 nm and the fluorescence decays were monitored at 620 nm at T = 25 °C. The relative fluorescence efficiency was calculated by $\varphi_{rel} = \frac{I_i/A_i^{405\,nm}}{I_{G65C}/A_{G65C}^{405\,nm}}$, where $I_i$ is the area under the fluorescence spectrum, $A_i^{405\,nm}$ is the absorbance at 405 nm for the sample. The values of $G_{60}$5Cur were chosen as reference for the other samples since it gave the highest $I_i/A_i^{405\,nm}$ -ratio.

**Table S10**. Maximum light absorption wavelengths and average fluorescence lifetimes <τ> for selected formulations.

| Formulation | $\lambda_{max}^{Abs}$ | <τ> (ns) |
|---|---|---|
| $G_{60}$2Cur | 430 | 0.155 |
| $G_{60}$5Cur | 432 | 0.201 |
| G2Cur | 425 | 0.105 |
| G5Cur | 428 | 0.170 |

| | | |
|---|---|---|
| B2Cur | 426 | 0.133 |
| B5Cur | 430 | 0.187 |

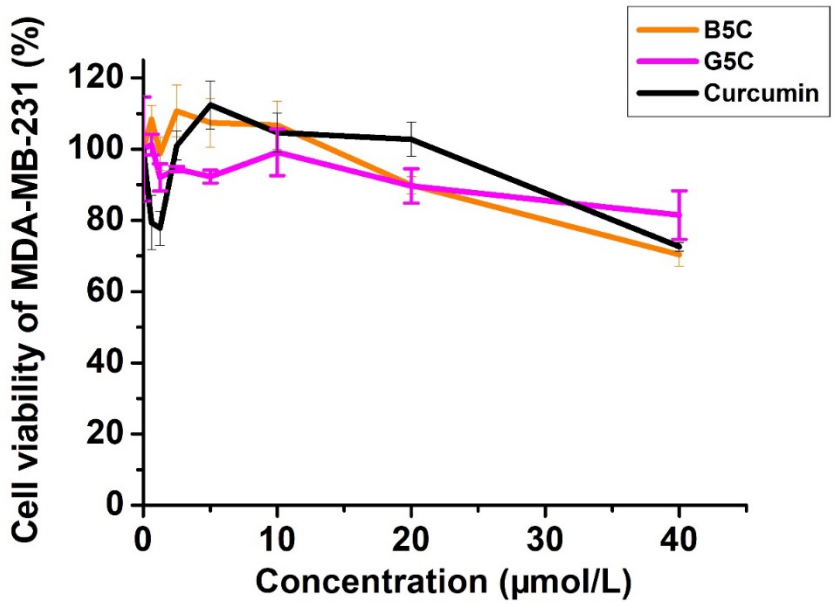


**Figure S9**. Viability of MDA-MB-231 cells after 48 h incubation with nanoformulations B5Cur and G5Cur. The concentrations refer to curcumin content.

**References:**

[1] Breßler, I.; Kohlbrecher, J.; Thünemann, A. F., *Journal of applied crystallography* **2015,** *48* (5), 1587-1598.

[2] Pedersen, J. S.; Gerstenberg, M. C., *Colloids and Surfaces A: Physicochemical and Engineering Aspects* **2003,** *213* (2-3), 175-187.

[3] Almgren, M.; Edwards, K.; Karlsson, G., *Colloids and Surfaces A: Physicochemical and Engineering Aspects* **2000,** *174* (1), 3-21. DOI https://doi.org/10.1016/S0927-7757(00)00516-1.